Evolving Starburst Modeling of FIR/sub-mm/mm Line Emission. II. Application to M 82

Lihong Yao

Department of Astronomy and Astrophysics, University of Toronto, Toronto, ON M5S 3H8, Canada

yao@astro.utoronto.ca

Submitted to ApJ on 15 March 2009; Accepted on 3 September 2009

ABSTRACT

We present starburst models for far-infrared/sub-millimeter/millimeter (FIR/sub-mm/mm) line emission of molecular and atomic gas in an evolving starburst region, which is treated as an ensemble of non-interacting hot bubbles which drive spherical shells of swept-up gas into a surrounding uniform gas medium. These bubbles and shells are driven by stellar winds and supernovae within massive star clusters formed during an instantaneous starburst. The underlying stellar radiation from the evolving clusters affects the properties and structure of photodissociation regions (PDRs) in the shells, and hence the spectral energy distributions (SEDs) of the molecular and atomic line emission from these swept-up shells and the associated parent giant molecular clouds (GMCs) contains a signature of the stage of evolution of the starburst.

The physical and chemical properties of the shells and their structure are computed using a a simple well known similarity solution for the shell expansion, a stellar population synthesis code, and a time-dependent PDR chemistry model. The SEDs for several molecular and atomic lines (^{12}CO and its isotope ^{13}CO, HCN, HCO$^+$, C, O, and C$^+$) are computed using a non-local thermodynamic equilibrium (non-LTE) line radiative transfer model.

By comparing our models with the available observed data of nearby infrared bright galaxies, especially M 82, we constrain the models and in the case of M 82, we provide estimates for the ages (5 - 6 Myr, 10 Myr) of recent starburst activity. We also derive a total H_2 gas mass of ~ 2 - 3.4×10^8 $M_\odot$ for the observed regions of the central 1 kpc starburst disk of M 82.

Subject headings: ISM: clouds – ISM: evolution – galaxies: ISM – galaxies: starburst – galaxies: star clusters – radio lines: ISM

1. Introduction

Knowledge of the physical properties and evolution of the gas and dust content in the interstellar medium (ISM) of starburst galaxies is essential for understanding the cause and temporal evolution of star-forming activity. In particular, studies of such galaxies in the nearby universe are essential as a step in understanding the role of the starburst phenomenon in the cosmic evolution of galaxies. To constrain theories of how the ISM evolves, one needs to investigate both individual galaxies and large statistical samples of data at multiple wavelengths. Especially, with the available data for the dust component, studying the gas in the co-space ISM becomes more interesting and important.

The number of multiwavelength observations of starburst galaxies throughout the cosmic-scale has increased dramatically due to the significant improvement in the sensitivity and resolution of telescopes. These observations provide an essential basis for starburst modeling, and such modeling provides systematic predictions of the properties of the ISM in idealized models of starburst galaxies for comparison with these observations. For example, M 82, an irregular starburst galaxy (*I0*) in the nearby universe has an inclination of 81°. The infrared luminosity of M 82 arises mostly from the central 1 kpc region, which has a stellar bar structure and a complex system of clumps and filaments (Lynds & Sandage 1963; Beck et al. 1978; Lo et al. 1987). The formation mechanism of this complex system and the evolutionary scheme in M 82 remain under debate (e.g. Visvanathan 1974; Carlstrom & Kronberg 1991; Shen & Lo 1996; Wills et al. 2000). Most recently, we conducted an ideal case study of an expanding shell model in M 82, and suggested that the circumnuclear rings seen in this galaxy may possibly be a consequence of the evolution of swept-up gas caused by starbursts that occurred in the center $\sim$ 100 Myr ago (Yao et al 2006, hereafter Paper I).

Previously, the age estimates of the starburst in M 82 have been presented by many authors. Yun et al. (1993) compared the disk HI with optical maps, and found a large amount of gas being channeled into the core of the galaxy over the last 200 Myr due to the tidal encounter with its large spiral neighbor galaxy M 81. Ages derived from super star clusters (SSCs) in optical and near-IR images are $\sim$ 50 Myr (de Grijs et al. 2001), $\sim$ 30 - 100 Myr (Rieke et al. 1993; Barker et al. 2008), $\sim$ 4 - 6, and 10 - 30 Myr (Förster-Schreiber et al. 2003; Smith et al. 2006; Melo et al. 2005). The corresponding estimates of the average star formation (SF) rate over the 200 Myr period is roughly about 10 $M_\odot$ yr^{-1}. The importance of optical and near-IR spectroscopy in studies of dusty star-forming galaxies has long been recognized. But studies of young stellar populations at these wavelengths remain difficult. The age determinations are affected by residual effects due to the age-metallicity degeneracy, and age-IMF degeneracy. In addition, the completeness of the sampled stellar population is affected by the unavoidable effects of extinction in the optical and near-IR.

The star formation history of M 82 has also been studied using mid-infrared and far-infrared spectroscopy (Colbert et al. 1999; Efstathiou et al. 2000; Galliano et al. 2003; Siebenmorgen & Krügel 2007). At these wavelengths, the fine structure line emissions are relatively insensitive to extinction, and hence can provide a unique probe of age and star formation history in an infrared-bright, dust-obscured galaxy like M 82. Colbert et al. (1999) obtained a burst age of 3 - 5 Myr for the central 1 kpc (65 - 85″) region using an instantaneous starburst model and a steady-state PDR model. However, their single burst model is dominated by the brightest and most recently formed stars (the hot spots seen in mid-IR). Efstathiou et al. (2000) presented an evolving starburst model for dusty media using state of the art codes for calculating the radiative transfer in dust shells, and incorporating a model for the composition and size distribution of grains in the ISM. Their study concluded that it is possible to relate the observed infrared spectrum of dust associated with a starburst to its age and its star formation history by following the evolution of an ensemble of GMCs of identical mass induced by massive star formation in their centers. They show that the burst age for the central 500 pc region of M 82 is between 10 and 30 Myr using a model with two instantaneous bursts. Their derived ages are supported by near-IR spectroscopy and high-resolution imaging of stellar clusters (Satyapal et al. 1997). Efstathiou et al. (2000) also suggested that far-IR surveys may preferentially detect older starbursts than mid-IR studies, based on an argument concerning the evolution of the luminosity of starbursts observed at different wavelengths. It is clear that the estimation of M 82 starburst age has a large uncertainty. The questions we ask are

Does the FIR/sub-mm/mm molecular and atomic line data contains a signal of the evolutionary phase of a starburst?

Can the molecular sub-mm and mm lines provide an alternative tool for estimating the starburst ages?

This study is motivated by the abundant evidence of giant bubbles and shells found in Milky Way, 30 Doradus in the Large Magellanic Cloud (LMC), and nearby starburst galaxies (Pedlar et al. 2003; de Grijs et al. 2001), the success of using the dusty starburst model to constrain the star formation history of observed IRAS starburst galaxies by following an ensemble of GMCs (Efstathiou et al. 2000), and the available multiple transitions in several molecular tracers. In a previous paper (Paper I), as a preliminary approach we presented a simple model of an expanding supershell surrounding a massive star cluster and its expansion at different evolutionary stages that predict sub-mm/mm and far-IR emission line intensities from several key molecular and atomic constituents in the shell (^{12}CO and its isotope ^{13}CO, HCN, HCO$^+$, C, O, and C$^+$). In this paper, we present a series of models,

called *Evolving Starburst Model* (ESbM) for the molecular and atomic line emission from an evolving starburst region, which is treated as an ensemble of evolving GMCs each of which is centrally illuminated by a compact star cluster (SC). The GMCs in our model ensemble follow a power-law mass spectrum. By comparing with the available observed data on nearby starburst galaxies, we can constrain the models and provide better interpretations for the observations. The main goals of this paper are (1) to show that it is possible to model the FIR/sub-mm/mm line emission of molecular and atomic gas by following the evolution of a starburst region, as in certain infrared (IR) models; (2) to relate the observed molecular line properties of a starburst galaxy to its age, and hence to constrain the global star formation history; (3) to understand the formation mechanism of the molecular rings in M 82; (4) and finally, to provide useful information for the interpretation of future high resolution maps of molecular gas on small and large scales in starburst galaxies, in order to provide a deeper understanding of the structure, dynamics, and evolution of the neutral ISM and its relationship with active star formation.

The plan of this paper is as follows. In § 2 we discuss briefly our model assumptions, initial parameters, and model procedure. In § 3 we present examples of our modeling results for an ensemble of GMCs/shells. In § 4 we present an application of the model to derive the age of the starburst and molecular gas swept up by the shells in M 82, and to provide new insights into the nature and physical state of the ISM in its starburst region. We also discuss applications to the supershell surrounding supernova remnant (SNR) 41.9 + 58. In the conclusions, we summarize the main results of this work.

Through this study, we hope to provide some answers to those intriguing questions mentioned above, and to lay a foundation for future starburst modeling for neutral gas media.

2. Evolving Starburst Model For Gas Media

The basic assumptions for our ESbM model are (1) star formation occurs within the dense optically thick spherical cloud (GMC) (e.g. Gao et al. 2001), and star formation takes place instantaneously, with the star cluster treated as a point source (see Paper I); (2) absorption of the starlight from the central cluster is produced by dust associated with the gas, assuming a constant gas-to-dust ratio; and (3) the gas responding to star formation in a starburst galaxy is treated as an ensemble of GMCs with different initial masses, each of which responds to massive star formation at its center.

Our ESbM model incorporates a standard similarity model for the bubble/shell struc-

ture around a young star cluster (Weaver er al. 1977; McCray & Kafatos 1987), a time-dependent stellar population synthesis model (Leitherer et al. 1999), a fully time-dependent chemistry model for the PDRs (Bell et al. 2005; Röllig et al. 2007), and a non-LTE radiative transfer model for molecular and atomic lines (Rawlings & Yates 2001; van Zadelhoff et al. 2002). Theoretical background for each of these four physics elements contained in our model has been presented in Paper I. Simulation methodology for an expanding supershell model has also been described in Paper I. In this paper we present an ensemble of ideal three-dimensional, spherical expanding shells, in order to model the line emission of neutral ISM in massive star-forming regions in a starburst galaxy like M 82. Our instantaneous starburst model does not address issues related to more complicated geometry in order to understand how these shells are distributed in a galaxy, how they interact, or how the gas becomes available for fueling the massive star formation in our model GMCs.

In this paper, we divide the evolutionary scheme of the expanding shell/GMC ensemble into two phases referred to as *Winds* and *post-SN*. The *Winds* phase begins with the formation of a star cluster and an H II region inside the GMC followed by the formation of a rapidly expanding hot bubble produced by strong stellar winds. This phase ends when the bubble breaks out of its parent GMC. In this phase, the parent GMC is assumed to be stationary, and acts as a dense uniform ambient ISM to the expanding shell formed by gas swept up by the bubble. The *post-SN* phase starts when the most massive star in the ensemble reaches its main-sequence lifetime, and explodes into a supernova. The shell expansion in this phase is first driven by repeated supernova explosions, then changes from pressure-driven (*adiabatic*) to zero pressure (*non-adiabatic*) as the hot bubble cools. In the *post-SN* phase, the shell expands into a less dense uniform ambient ISM. A steady-state mechanical power and energy for each phase is assumed, in order to satisfy the requirements of the similarity model. Our non-LTE line radiative transfer method simply sums the line emission from the model shells and parent GMCs in the ensemble for the *Winds* phase, and just the model shells for the *post-SN* phase. Hence, our model is an idealistic approximation for a starburst galaxy; it may be considered the first step toward simulating the response of the gas environment in an evolving starburst region for the purpose of examining the effects of this evolution.

A schematic diagram of the model components (PDR or shell and its parent GMC) is shown in Fig. 1. In this paper, we treat the PDR and shell as one gas component. The line intensity/flux for the shell and GMC components are calculated using the same method. For the *Winds* phase, the integrated line intensity/flux at each time step is the sum of line emission in the shell and its parent cloud. For the *post-SN* phase, the integrated line intensity/flux is the emission from the shell only. Due to the incomplete knowledge of the structure and physical state of the ambient ISM in a starburst galaxy, we do not include the molecular or atomic line emission from this component in our model. The justification of the

ambient ISM density (30 cm^{-3}) will be discussed in § 2.2.2. In § 4, we discuss the possible impact of this exclusion on the conclusions, specifically regarding the applications to M 82.

2.1. Model Outline

Our basic model comprises a series of non-overlapping (i.e. non-interacting) spherical shells expanding into a uniform gas medium. These shells are all driven by winds from star clusters formed during an instantaneous starburst. The interior hot bubble is produced by stellar wind from an underlying super star cluster, whose properties are selected as discussed later. The thrust of our model simulation is to compute the molecular line emission from the swept-up shells and the associated parent GMCs. Since the underlying stellar radiation from the clusters has a pronounced effect on the properties of PDR regions of the shells, and since these properties are therefore also affected by the radius of the shell and evolutionary stage of the cluster, the SED of the molecular line emission from these shells contains a *signature* of the stage of evolution of the starburst. This variation with time, predicted by our model, offers a way of dating the starburst, at least in principle.

The set of our starburst models is divided into two phases, namely the *Winds* and *post-SN* phases. In the *Winds* phase, the shells propagate into their parent clouds, which are substantially more dense than the surrounding ISM in which they are embedded. In the *post-SN* phase, the shell breaks out of the parent cloud and expands into the uniform lower density ISM which pervades the entire galaxy. The same bubble/shell dynamical theory is used to describe the shell behavior in both phases. Since the simple similarity relations do not apply to a nonuniform ambient medium, we do not follow the shell expansion across the transition from cloud to the surrounding ISM. Instead the two phases are treated independently, and can be viewed as simply alternative scenarios. Continuity at the transition is only maintained in the mechanical luminosity of the wind (L_w) and the stellar luminosity (L_*) evolution of the central star clusters. There is accordingly a *discontinuity* in the radius (R_s), velocity (V_s), and consequently the temperature (T_s), density (n_s), thickness (d_s), and the mass of each expanding shell across the boundary between the two phases. These quantities asymptotically approach those of a continuous model when the mass of the ISM swept up in the *post-SN* phase becomes greater than the mass of the parent GMC in the *Winds* phase. The *Winds* phase thus comprises younger and denser shells than in the *post-SN* phase. In principle, it is possible to model data with starbursts occupying a large range of potential ages and molecular gas excitation conditions, especially if the dense molecular core component were also included our model. For this study, our *Winds* phase model results are used only for a comparison with the observed expanding supershell surrounding SNR 41.9 + 58 in the

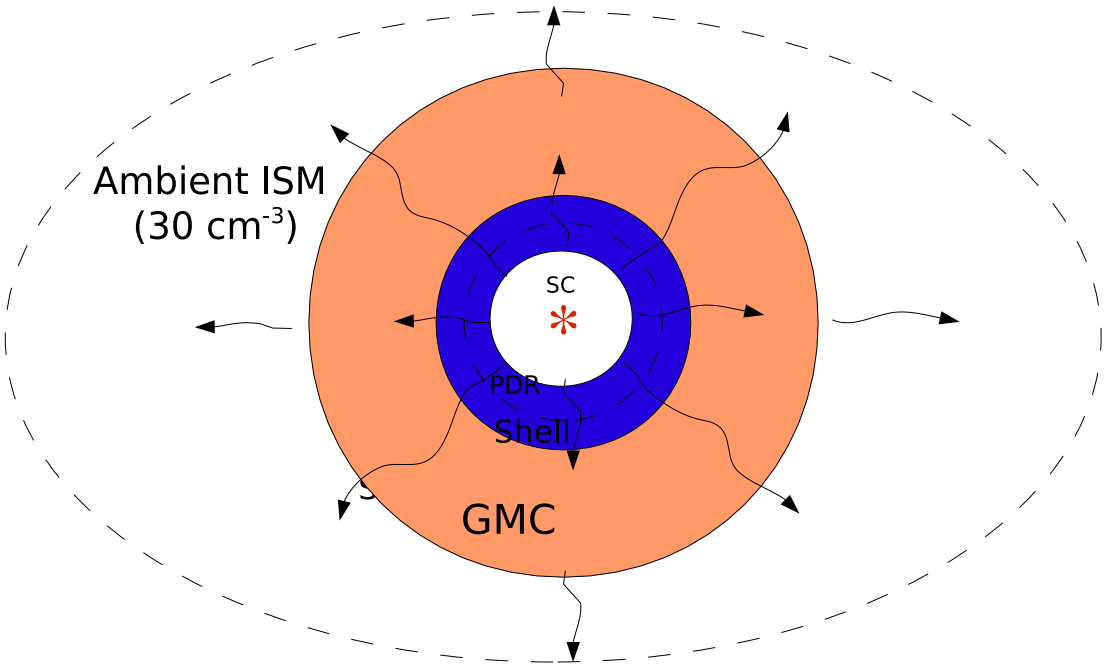

Fig. 1.— This diagram illustrates the structural components associated with a single star cluster within our model. The white region is the hot cluster wind, the blue region is the shell of material swept up from the giant molecular cloud, represented by the orange region. The region exterior to the GMC is the ambient interstellar medium (ISM) with a fixed H_2 density of 30 cm^{-3}.

center of M 82, which will be discussed later in § 4.

In each phase, the shell structure is computed with time as the independent variable. The final output dependent variables are the line fluxes (and profiles) for several molecules and atoms each at a number of observed transitions, computed by a non-LTE line radiative transfer code applied to each shell and its parent cloud. The integrated line flux for each shell (and GMC) is the sum over the emission from the entire emitting region. The total line flux for the shell ensemble is then the sum of the integrated line fluxes of all shells (and GMCs). Intermediate variables which determine these fluxes include the radius and velocity of each shell, its chemical structure, shell temperature and density structure, which are computed using a *Shell Dynamics* code, a stellar population synthesis code, and a time-dependent PDR code. These codes are described in detail in the *Ph.D. Thesis* of Yao (2009, hereafter Yao Thesis, and references therein).

Our two-phase starburst model described above must also be characterized by a number of fixed parameters with adopted plausible values. These include, for example, the initial giant molecular cloud parameters (mass M_{GMC}, initial H_2 density n_0, and core H_2 density n_c), the star formation efficiency (η), the star cluster related parameters (IMF, individual star mass m_*), the initial chemical composition of the parent clouds, and the density of the ambient ISM. These parameters, along with others, and their numerical values, are discussed in detail in the subsequent sections, in association with the discussion of the PDR and radiative transfer codes. A brief summary of all variables and parameters are presented in Table 3 at the end of this section.

Finally, a chi-square (χ^2) method will be used for fitting the model line spectral energy distribution to a set of molecular line data in order to estimate the starburst age(s) and observed total H_2 mass in the nuclear disk of M 82. In a subsequent paper (Yao 2009), we will present applications to luminous infrared galaxies (LIRGs) (e.g. Yao et al. 2003) beyond M 82 using our FIR/sub-mm/mm starburst model. We discuss the relationships between the excitation of CO molecule and SF properties of LIRG galaxies, and derive the behavior of the model CO-to-H2 conversion factor X in a starburst galaxy.

2.2. Model Input Parameters

2.2.1. Winds Phase

In 2005 Keto et al. observed ^{12}CO(2-1) emission in the center of M 82 with a linear resolution of 17 pc at the source. They resolved ~ 300 molecular clouds with masses ranging from $\sim 2 \times 10^3$ to 2×10^6 $M_\odot$. The mass spectrum of these GMCs scales as dN/dM_{GMC}

$\propto M_{GMC}^{-1.5\pm0.1}$, similar to the Galactic one (Sanders et al. 1985; Solomon et al. 1987). Keto et al. also found that the mass spectrum of star clusters in M 82 follow the same power-law distribution, suggesting that individual molecular clouds are transformed in the starburst into individual star clusters in their dense cores. Combining this result with other studies (e.g. Weiss et al. 2005), we assume the GMC mass distribution responsible for the stellar outburst in our model has a power-law index of 1.5, and the mass ranges between 3.16×10^3 and 10^7 $M_\odot$. About 70% of molecular gas mass in a model starburst will then be contained in the clouds with masses $> 10^6$ $M_\odot$. It is also expected that much of the FIR luminosity due to star formation would arise from these massive clouds. To reduce the computation time, a discrete and arbitrary number of giant molecular clouds distributed similar to that discussed in Keto et al. (2005) is assumed. The masses for these discrete GMCs are 3.16×10^3, 10^4, 3.16×10^4, 10^5, 3.16×10^5, 10^6, 3.16×10^6, and 10^7 $M_\odot$, and are hereafter denoted as 3M3, M4, 3M4, M5, 3M5, M6, 3M6, and M7. The total number of clouds is about $\sim$ 400, and the total H_2 mass contained in the GMCs and shells is $\sim 1.69 \times 10^7$ $M_\odot$ with a total star clusters mass of 4.2×10^6 $M_\odot$. This selection is intended to provide a template cloud/cluster mass for scaling the model to fit the data for M 82. The best fitting molecular H_2 gas mass and the initial star cluster mass will be determined from a χ^2 fitting method, as described later in § 4.

The average gas densities of GMCs in our Galaxy and starburst galaxies are in the range a few 10 to a few times 10^2 cm^{-3} (Dame et al. 1986; Jog & Solomon 1992; Wilson et al. 2008), but their cores, where most of the stars form, have much higher densities. Higher gas densities are expected in more actively star-forming galaxies in accordance with the Schmidt law (Kennicutt 1998). Therefore, we adopt a value of 300 cm^{-3} for the uniform initial H_2 gas density (i.e. n_0) for the M7 cloud based on the densities for the most massive clouds in the study of molecular cloud properties in the active spiral M 51 by Scoville & Wilson (2004). Since this work is proposed to be a complementary study to the dusty starburst models developed by Efstathiou et al. (2000), we adopt the same core density namely $n_c = 2 \times 10^3$ cm^{-3} for the calculations of the number of ionizing photons (used in computing the Strömgren radius R_S value). The radius of this 10^7 $M_\odot$ cloud is 47 pc derived from the mass of the cloud and the assumed density with the assumed effective molecular weight $\mu = 2.36$ (e.g. Elmegreen et al. 1979; McCray & Kafatos 1987).

We know that star formation takes place primarily in the dense cores of GMCs, but the details of the physical processes involved are not yet well understood. The efficiency of star formation (or the gas consumption rate) ranges from about 1% in late-type spirals to 60% or more in active star-forming galaxies (Kennicutt 1998). In this paper we adopt a moderate star formation efficiency $\eta = 25\%$ for our model starburst galaxies. A Salpeter IMF is assumed, i.e. $dN/dm_* \propto m_*^{-2.35}$ (IMF; Salpeter 1955), and the stellar mass is in the

range 0.1 - 120 $M_\odot$.

We assume that the relationship between cloud mass and radius is the same as that derived from a CO survey for 273 giant molecular clouds in the Galactic inner disk by Solomon et al. (1987). From the measured relationship between the cloud size and the velocity line width, and the application of the virial theorem, they derived a power-law cloud density and mass relation, in which the mean gas density of the cloud is inversely proportional to the cloud size. Hence, the cloud mass is proportional to the square of the cloud radius (i.e. the mass surface density is a constant). From the studies of independent methods of determining the H_2 mass, Solomon et al. (1987) also demonstrated that these giant molecular clouds are bound principally by self-gravity and not by external pressure exerted by a hot phase of the ISM. Since we assume the mass distribution of GMCs in a starburst galaxy is similar to that in our Galaxy, we adopted the power-law relations of mass, radius, and density for our model GMCs as those defined in Solomon et al. (1987). This mass - radius relation has also been studied for GMCs in other galaxies, for example M 51 by Bastian et al. (2005), and has been found to be similar in form. Hence, the density and the radius for a model GMC having mass less than 10^7 $M_\odot$ can be written in the following forms,

$$n_0 = 300\ cm^{-3} \times \left(\frac{R_{GMC}}{47\ pc}\right)^{-1}, \quad (1)$$

$$R_{GMC} = 47\ pc \times \left(\frac{M_{GMC}}{10^7\ M_\odot}\right)^{\frac{1}{2}} \quad (2)$$

where R_{GMC} is the radius of the GMC with mass M_{GMC} that is less than 10^7 $M_\odot$. Table 1 summarizes the number distribution of the GMCs and their initial physical properties. For GMC mass less than 3.16×10^3 $M_\odot$, the predicted number of very massive stars (> 30 $M_\odot$) in the star cluster is below 1.0. In addition the supernova wind will not be steady as assumed in our model, because of the relatively small numbers of contributing stars. Initially, the total GMC and cluster masses are assumed to be $\sim 1.86 \times 10^7$ $M_\odot$ and $\sim 4.27 \times 10^6$ $M_\odot$, respectively.

2.2.2. Post-SN Phase

All shells are propelled into a less dense ambient ISM during the *post-SN* phase. The intercloud medium of the central 1 kpc region of the Galaxy has been studied by Jog & Solomon (1992), who find it to be mostly molecular with density between 30 and 100 cm^{-3}.

Table 1. Initial conditions of GMCs and SCs in a modeling starburst system.

GMC (N_{norm})[a]	$\log_{10}M_{GMC}$[b] ($M_\odot$)	n_0[c] (cm^{-3})	n_c[d] (cm^{-3})	R_{GMC}[e] (pc)	$\log_{10}M_{SC}$[f] ($M_\odot$)	($0.1M_\odot \leq M_* \leq 120M_\odot$)	N_*[g] ($M_* \geq 8M_\odot$)	($M_* \geq 30M_\odot$)	$\log_{10}L^*_{SC}$[h] (erg s^{-1})	$\log_{10}L^{mech}_{SC}$[i] (erg s^{-1})
M7 (1.0)	7.0	300	2000	46.8	6.4	7.1E6	2.2E4	5.0E3	42.8	40.1
3M6 (1.77)	6.5	534	3558	26.3	5.9	2.2E6	7.0E3	1.6E3	42.3	39.6
M6 (3.1)	6.0	949	6325	14.8	5.3	7.1E5	2.2E3	5.0E2	41.8	39.1
3M5 (5.6)	5.5	1688	11251	8.3	4.9	2.2E5	7.0E2	1.6E2	41.3	38.6
M5 (10.0)	5.0	3000	20000	4.7	4.4	7.1E4	2.2E2	50.0	40.8	38.1
3M4 (17.7)	4.5	5337	35578	2.6	3.9	2.2E4	70.0	15.0	40.3	37.6
M4 (31.6)	4.0	9487	63246	1.5	3.4	7.1E3	22.0	5.0	39.9	37.2
3M3 (56.2)	3.5	16876	112509	0.8	2.9	2.2E3	7.0	1.0	39.4	36.7
Ensemble (127)	7.27	···	···	···	6.63	1.57E7	4.9E4	1.1E4	43.1	···

Note. — All data listed in the above table are for single SC, except for the Ensemble.

[a]GMC type (number of GMC in an ensemble).

[b]GMC mass.

[c]Average gas density of a GMC.

[d]GMC core density.

[e]GMC radius.

[f]Star cluster mass.

[g]Star number for different stellar mass ranges.

[h]Stellar bolometric luminosity.

[i]Mechanical luminosity (Stellar wind + SN).

Bally et al. (1988) also obtained an average molecular gas density of 50 cm^{-3} for the region within a radius of 500 pc of the center of our Galaxy. In this paper, we assume a uniform ambient ISM with similar density surrounding the GMCs for our model.

To investigate whether this medium should be considered as atomic or molecular, and to get an estimate of its mean density, we compare the observational constraints for various ambient ISM constituents (H_2, HI, and H II) for the central 1 kpc region of M 82. Table 2 shows that gas with a column density of about 10^{23} cm^{-2} is required by observations, and that the dominant state of the ISM is molecular. Hence, from this observed H_2 column density, and an adopted diameter of 1 kpc for the starburst region, we can derive the number H_2 density of about 30 cm^{-3} (or a total H_2 mass of $\sim 1.2 \times 10^9$ $M_\odot$), and we adopt this figure for modeling the central 1 kpc region in M 82.

In reality, intercloud gas in M 82 is unlikely to be uniformly distributed, as assumed in our model. Recent studies (e.g. Glover & Mac Low 2007, and references therein) show that a smoothly distributed turbulent medium consisting of atomic gas would quickly (within a few 10^6 yr) develop density fluctuations, becoming a highly non-uniform medium of molecular H_2, with density enhancements up to a factor of 100 or more times the mean density. For simplicity, we ignore these density fluctuations, and regard this medium as represented by its mean density, treating it as uniform for the purpose of computing the material swept-up by the expanding shells.

The standard input parameters in our time-dependent PDR simulation that describe the physical properties of the model shell were summarized in Table 2 of Paper I. The cosmic-ray ionization rate ζ adopted in this paper (the standard Galactic value, i.e. 1.3 - 2.0 $\times$ 10^{-17} s^{-1}) is up to two orders of magnitude lower than that measured in M 82 (e.g. Farquhar et al. 1994). However, the main heating mechanisms of the PDRs are photoelectric, H_2 FUV pumping, and H_2 photodissociation. The contribution to the total heating rate from cosmic-ray ionization and excitation and the decay of turbulence within the cloud/shell is generally

Table 2. Observed column density of various ISM components in the center of M82.

Type	Column Density (cm^{-2})	Reference
H_2	6.1×10^{22}	Wild et al. (1992)
	a few $\times$ 10^{23}	Mao et al. (2000)
HI	2.6×10^{22}	Weliachew et al. (1984)
H II	9.0×10^{22}	Carlstrom & Kronberg (1991)

negligible. These processes only become important at large depths during late starburst evolution and/or dark cloud (Bell 2006).

The input parameters for a single-point dense dark-cloud model, which is used to produce the initial abundances at the first time step ($t = 0$ yr) all depth steps for our PDR simulation, were also described in Paper I. The dark-cloud assumption of chemistry is the same for all depth steps; it is a reasonable guess for the initial gas conditions in a GMC before star formation occurs. Our starburst model time step begins at $t = 1.0 \times 10^4$ yr, adopted as the time when the massive star formation occurs in the center of the GMC. For this time step and the subsequent time steps, the input abundances are re-set to the output abundances of the previous time step generated by the *UCL_PDR* code. The chemistry at first iteration is calculated from gas temperature and attenuated FUV flux, and then revised iteratively until the balance criteria of heating and cooling is reached for each depth step at each time step. Hence, the final results are not significantly dependent on our initial dark cloud chemistry input at $t = 0$ yr. The metallicity dependence appears in several key processes in the our PDR calculations, and accordingly we adopt solar abundances for the metals, i.e. unit metallicity. The dust-to-gas mass ratio is adopted as 1/100. Standard values of dust properties are used in the model (see Table 2.3 in Bell 2006), though the *UCL_PDR* code allows the various dust properties to be specified as free parameters which can vary with shell depth and time.

The chemistry within the parent GMC outside the shell is also handled by the same PDR analysis, using the different (lower) density in this region. The incident FUV strength for the cloud region is the attenuated radiation field emerging from the outer boundary of the shell, and the FUV strength inside the cloud is computed in the same way as for the shell, with the computation of A_V taking account of the lower density of the dust.

Our multi-level non-LTE radiative transfer *SMMOL* code includes an empirical dust extinction model (see Table 1 in Mathis 1990). In our models, we assume the entire region containing all of the shells is unresolved. The lowest ten energy levels are incorporated for molecular species (CO, HCN, HCO^+, CN, HNC), three levels for atomic [C I] and [O I], and two levels for atomic [C II]. In Paper I, single collisional partner (H_2) was used in the radiative transfer calculations. In this paper, multiple collisional partners (H, e^-, H^+, p-H_2, o-H_2, He) are taken into account in the statistical equilibrium equation calculation. The collisional excitation of molecular lines involves two partners, i.e. p-H_2 and o-H_2, but the excitation of [C I] fine structure lines is affected by collisions with all six particles, five (without He) for [O I] lines, and four (without He and H^+) for [C II] lines. Since these forbidden lines have very low radiative transition probabilities, the upper states are populated primarily by collisions, and they are usually optically thin.

The input parameters to the *SMMOL* model are (1) molecular data including molecular mass, energy levels, transition frequencies, radiative rates and collisional rates; and (2) physical data describing the object to model. This includes the physical distance of the current grid point to the center of the shell, gas density, number densities of the six collisional partners (H, e^-, H^+, p-H_2, o-H_2, He), the fractional abundance of molecules or atoms, the gas (kinetic) and dust (thermal) temperatures, shell expansion velocity, and the microturbulent velocity.

Table 3 summarizes the parameters and variables used in our simulations.

3. Model Results

In this section we present examples of our simulation results for the shell ensemble centrally illuminated by massive star clusters. Detailed results for individual expanding shells can be found in Yao et al. (2006) and Yao Thesis. These shells are modeled in a similar way for both *Winds* and *post-SN* phases as described in previous sections. A family of these evolving shells form the basis of our starburst models in accordance with our description in § 2. Applications of the shell ensemble to M 82 and more distant starburst galaxies will be presented in subsequent sections.

The two modeling phases are indicated by *Winds* and *post-SN* labels in tables and plots throughout the remainder of this paper.

3.1. Kinematics of The Swept-up Gas

The strong stellar winds and supernova explosions from hundreds to thousands of the massive stars fuel the hot bubbles over a timescale > 10 Myr. The kinetic energy in the supersonic wind is thermalized by a stand-off shock, and the high pressure downstream drives a strong shock into the ambient ISM. The swept-up gas condenses into a narrow shell as a result of radiative cooling. The wind mechanical luminosity E_{mech} comes mainly from Wolf-Rayet (WR) stars, with some contribution from O stars. All other stars produce a negligible effect.

During the *Winds* phase, the sizes of the initial Strömgren spheres in our model ensemble increase slowly with time. The Strömgren radius ranges from 0.02 to 4.9 pc with the number of Lyman continuum photons between 1.5×10^{49} and 5×10^{52} s^{-1} generated from the central star clusters derived from Equation (2) in Efstathiou et al. (2000). The wind bubble catches up with the ionization front of the compressed shell in a time less than 10^5 yr. The strong

stellar winds cause the bubbles to expand quickly into their parent clouds and to sweep up more gas into the shells. When the most massive star in the most massive star cluster (i.e. 120 $M_\odot$ star in the M7 cloud) terminates as a supernova at ~ 0.8 Myr (Mac Low & McCray 1988), this marks the beginning of *post-SN* phase. At this time, the largest thin shell (M7) caused by the stellar winds is expanding at a speed of ~ 50 km s^{-1}, and all the shells have swept up the material in their parent clouds. The *Winds* phase ends earlier (< 0.8 Myr) for shells smaller than that for the M7 cloud. After 0.8 Myr, the shells begin to expand into a less dense uniform ambient ISM (i.e. 30 cm^{-3}). The mechanical energy produced by the first supernova and the subsequent ones re-energizes the shell formed in the *Winds* phase.

The hot bubbles begin to cool at ~ 0.8 Myr for the 3M3 shell and ~ 7.5 Myr for the M7 shell. At this time, the radius and velocity of the M7 shell are about 270 pc and 24 km s^{-1}, respectively. After this time, the superbubbles start to lose their internal pressure, and the shell expansion velocity decreases rapidly. When the shell velocity approaches the sound speed of the ambient ISM, the shells should stall and become thicker and less dense. The latter effect is not included in our model, since the external pressure of the ISM is ignored. It is clear that the lifetime of the progenitor GMCs may be short, but the birth of massive star clusters and their impact on the surrounding ISM is profound.

In addition, we calculate the total amount of gas M_{model} in our model GMC/shell ensemble following the evolution of the shells, as shown in Fig. 2. The discontinuity seen at 1 Myr is caused by the phase change (*Winds* to *post-SN*), in which the parent GMC mass contained in the shell is no longer taken into account after the shell sweeps up all material in its parent GMC. This mass will be used as a template or reference value to be scaled to the total H_2 gas mass in a observed region of M 82 using a χ^2 analysis for our model line SEDs, under the assumption that the line flux in the measured region is proportional to the total molecular gas mass (see § 4 for details).

3.2. Thermal Properties and Chemistry of the PDRs

Over the 100 Myr of shell evolution the total mechanical wind power produced by individual cluster varies greatly, for example, from 10^{34} - 10^{40} erg s^{-1} for the most massive cluster in our model ensemble. In this paper, the mechanical power profile is used only for obtaining average values over each phase in order to compute the shell dynamics. The kinetic energy of the shells is between 10^{43} ergs and 10^{54} ergs, depending on cluster mass. The FUV radiation incident on the inner surface of the shells ($A_V = 0$) is a function of time ($G_0 \propto R_s^{-2}$; see in Paper I). The G_0 value is in units of the Habing field (1.6×10^{-3} ergs cm^{-2} s^{-1}) throughout this paper. This value decreases from about 10^6 - 10^8 (depending on

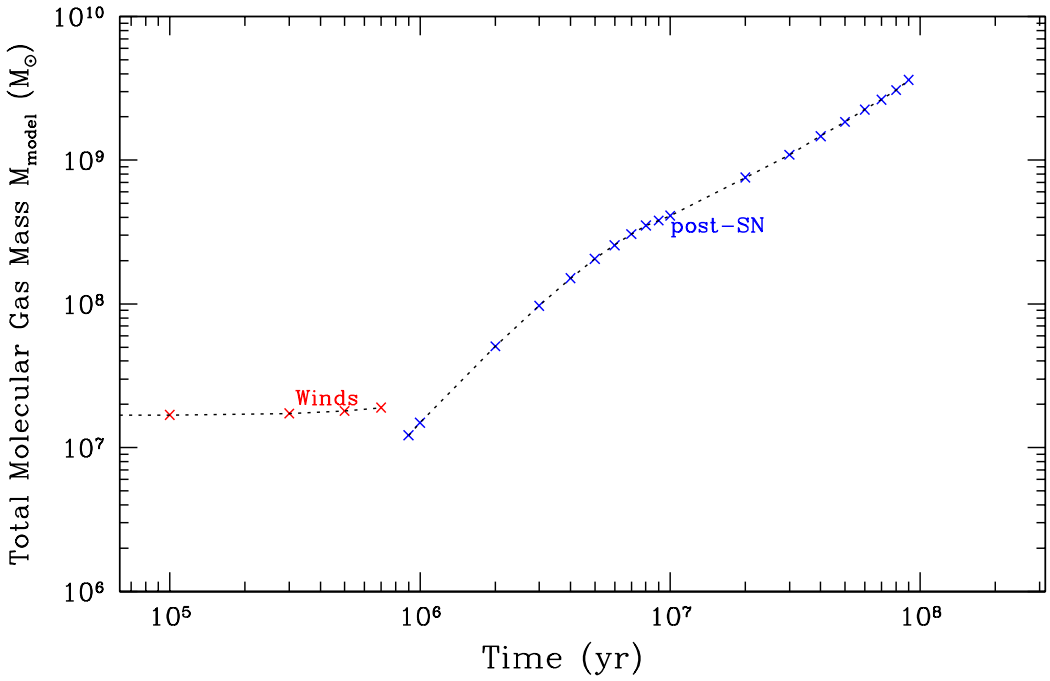

Fig. 2.— Plot of the total H_2 mass swept-up by the shells and the mass remained in parent GMCs (*Winds* phase only) as a function of time.

cluster mass) at the onset of massive star formation (i.e. $t = 0$ yr) to between 10^2 and 10^5 respectively at 5 Myr when most of the massive stars ($M_* > 30$ $M_\odot$) reach the end of their lifetime. At $t = 100$ Myr, the G_0 values drop by 4 - 5 orders of magnitude.

3.2.1. Density and Temperature

The shell density, thickness, and temperature are calculated for both *Winds* and *post-SN* phases. Fig. 3 shows an example of simulation results of an M7 shell. The density value varies from 10^2 to 10^6 cm^{-3} and the thickness is between 10^{-3} and ~ 10 pc over a 100 Myr period, depending on cluster mass. The *plateaus* seen at the beginning of the *Winds* phase are due to small changes in the expansion velocity and shell temperature. Before the shell sweeps up all of the material in its parent cloud ($t < 0.8$ Myr), the shell density declines with increasing shell radius and decreasing shell velocity, and the shell thickness increases with time. The dense phase of the shells (10^4 - 10^6 cm^{-3}) is very short lived (between 10^4 - 10^6 yr). After the first supernova occurs (i.e. *post-SN* phase), the bubble continues expanding adiabatically into a lower density ambient ISM until a time t_c (indicated in the plots), when this hot interior begins to cool and the shell enters the *snow-plow* phase while conserving its total momentum. The shell velocity then decreases rapidly with a corresponding decrease in shell density, to about three orders of magnitude lower than that at the *adiabatic* phase. Such large variation in the shell density is due to the range of dynamic pressure produced by the range in the shell expansion speed. The shell thickness increases from 0.1 pc at the beginning of the *post-SN* phase to 10 pc at 100 Myr. Similarly, the thickness covers a large range because in the early phases, the shells are highly compressed and contain very little mass, so they are thin compared to later phases where these conditions are reversed.

In the plot, the first big jump occurs when the wind shock front catches up with the ionization front, and the expansion changes from H II to wind driven. For smaller GMCs, this transition takes place in less than 10^3 yr. The discontinuity (or gap) between *Winds* and *post-SN* phases is due to the model change from *Winds* to *post-SN* phase. A smaller jump is also seen when radiative cooling inside the bubble becomes dominant, the shell switches from the *adiabatic* to the zero pressure *snow-plow* phase.

Fig. 4 shows an example of the gas and dust temperatures as a function of the visual extinction A_V for an M7 shell at different starburst ages. The A_V is set to be 0 at the inner surface of the shell (i.e. boundary between the hot bubble and the shell), and increases toward the outer edge of the shell (i.e. boundary between the shell and its parent cloud or the ambient ISM). During the *Winds* phase, the cloud A_V progresses from the outer edge of the shell to the outer edge of the GMC (i.e. boundary between the GMC and its

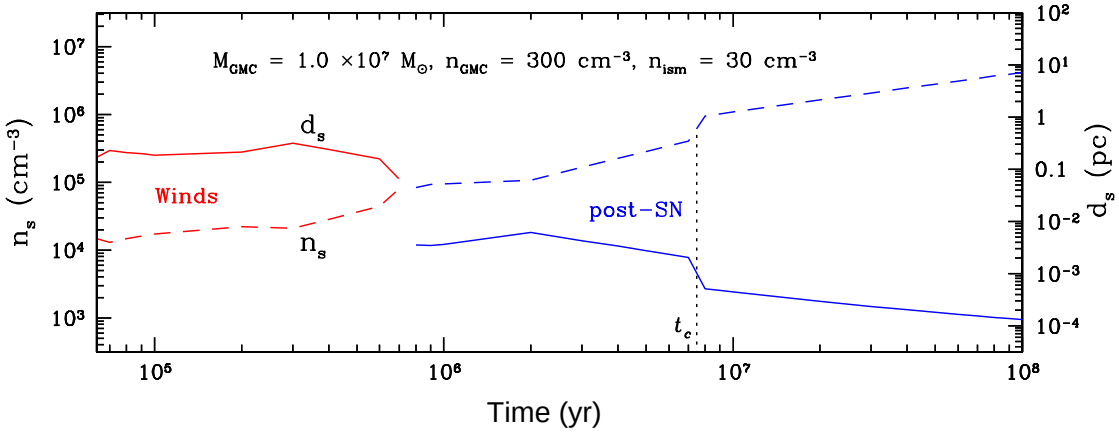

Fig. 3.— Plot of the density (n_s, solid line) and thickness (d_s, dashed line) of an M7 shell as a function of time. The *Winds* phase is indicated by red curves, while the *post-SN* phase is indicated by blue curves. The radiative cooling of the hot interior occurs at t_c indicated by the dotted lines.

ambient ISM). The gas temperature has a negative gradient from the inner edges of the shells to the outer edges, because the FUV flux is attenuated owing to dust extinction resulting in decreasing photoelectric heating across the shells. The FUV field strength $G(t, A_V)$ at different A_V (or depth in the shell) is a factor of $e^{-1.38A_V}$ less than the flux at the surface of the PDR (or G_0). For example, at 1 Myr the FUV field strength at $A_V = 2$ (layer of C^+/C/CO transition) is attenuated to $\sim 6\%$ of the value at the surface ($G_0 \sim 10^3$ - 10^6) for the shells in the ensemble. The gas temperature is in the range 10 - 1000 K across the shells. It is about 1 - 2 orders of magnitude higher than the dust temperature at the surface of the PDRs. Fig. 5 shows an example of the temperature structure for an M7 cloud before the shell sweeps up all of its materials. The parent cloud is also heated by FUV radiation from the central star cluster. The minimum A_V for the GMC corresponds to the extinction due to the shell at the shell-cloud interface, and the maximum A_V is the extinction at the outer edge of the cloud. The gas temperature changes from 1000 K to about 10 K across the clouds, it drops rapidly with A_V once the FUV field is attenuated, reaches a minimum when the CO cooling is most efficient. But when the gas becomes optically thick toward the outer edge of the parent GMC, the gas temperature rises slightly with increasing A_V (e.g. age beyond 0.3 Myr) due to the assumption of a semi-infinite slab used in our PDR model. Since the cooling line emission does not escape from the outer edge of the GMC, the cooling of the gas is inhibited. This causes an increase in the equilibrium gas temperature at large A_V. Although this effect is nonphysical, it affects only our *Winds* model, and it has no effect on the *post-SN* phase, and thereby no effect on our derived age discussed later in § 4.

Although the physical properties of each giant molecular cloud and the star cluster born in its center vary greatly with cluster and cloud mass, the model profiles for the shell density, thickness and temperature are similar. This implies that different initial cloud conditions in a starburst environment may yield similar gas properties through the entire evolution. However, for individual shells, the physical properties of gas inside the shells change drastically with time. These gas properties that contain the imprint of different evolutionary phases, also determine the molecular line radiative transfer, and hence the spectral energy distribution of line fluxes. It allows us in principle to date the burst age by modeling the line spectrum energy distribution for various molecular tracers and comparing them with the observations of a starburst galaxy.

3.2.2. Chemical Evolution

The chemical structure inside the shell is stratified. The FUV photons are gradually absorbed and lead to relatively sharp transitions. In Fig. 6, the transitions of atomic species

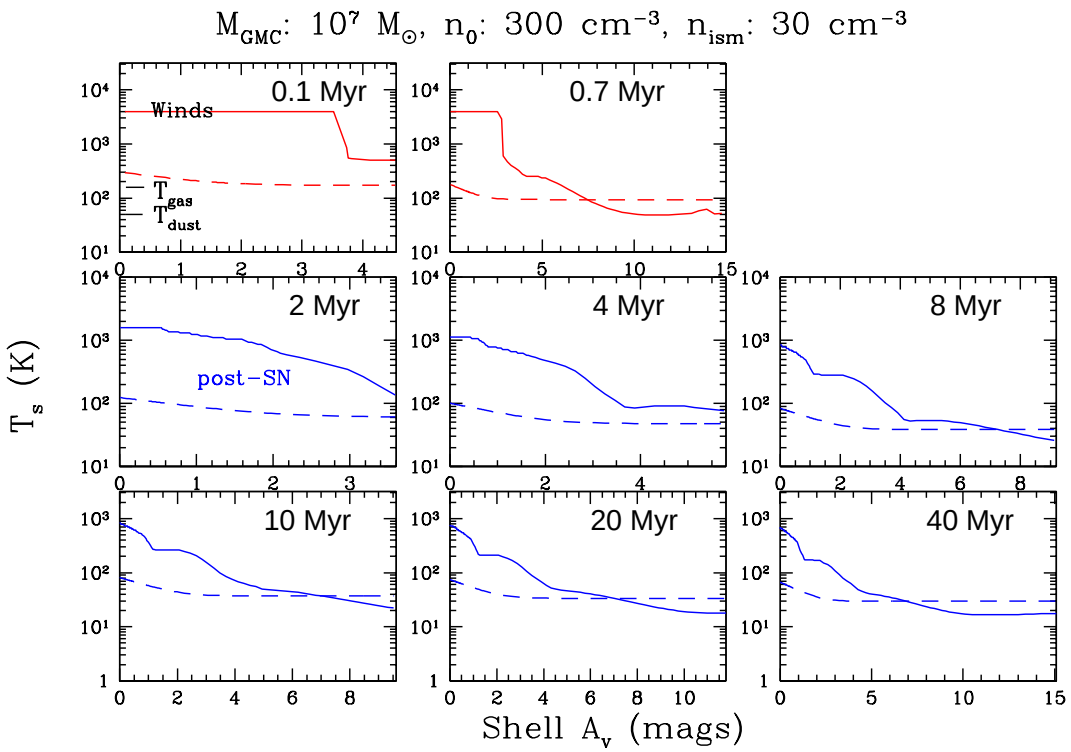

Fig. 4.— Plot of the time-dependent gas and dust temperatures as a function of visual extinction A_V for a M7 shell. Solid lines represent gas temperature, and dashed lines indicate dust temperature. The *Winds* phase model is indicated by red curves, and the *post-SN* phase model is indicated by blue curves.

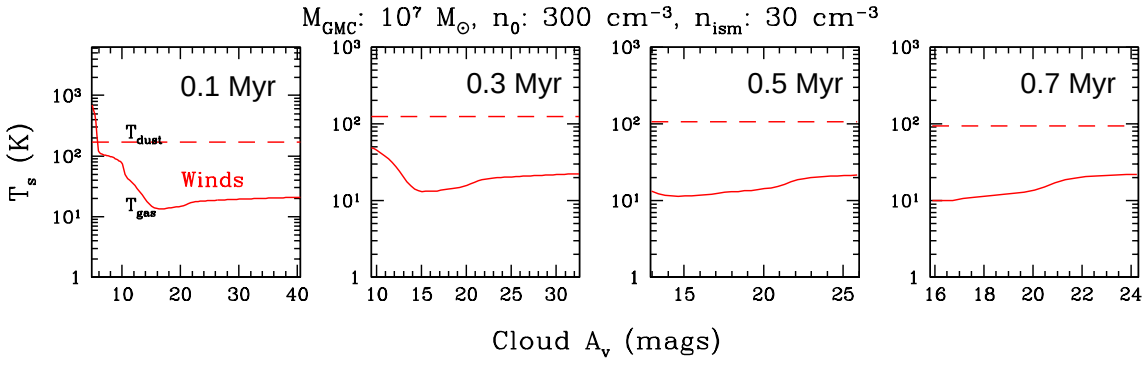

Fig. 5.— Plot of the time-dependent gas and dust temperatures in the parent GMC (M7 cloud) as a function of visual extinction A_V. Solid lines represent gas temperature, and dashed lines indicate dust temperature.

(H^+/H, C^+/C, O) to molecular gas (H_2 and CO) in an M7 shell are shown. The H_2 abundance becomes much more enhanced at $A_V > 1$, and the formation of CO occurs at $A_V = 3$ - 4. At the surfaces of the shells, the dominant coolant is the [O I] 63 μm fine-structure line. Deeper into the shells and the clouds the cooling by [C II] 158 μm, [C I] 610 μm, and CO becomes dominant (not shown). The chemical structure inside the shells changes significantly for the first few million years. This further justifies the use of a time-dependent PDR model for our shell evolutionary models. Figs. 7 shows the chemical evolution inside an M7 cloud, before the shell sweeps up all of its material.

3.3. FIR/sub-mm/mm Line Emission in Individual Shells and A Shell Ensemble

3.3.1. ^{12}CO and Its Isotope ^{13}CO

Fig. 8 shows our model ^{12}CO line SEDs ($J = 1...9$) as a function of the starburst age for a single shell (corresponding to the M7 GMC) and a shell ensemble. In plot (a) the total line flux S_{CO} is summed from gas in one single expanding shell and its parent GMC with a mass of 10^7 $M_\odot$ (M7 GMC and Shell or SS model). The parent GMCs contribute significantly to the total lower-J line emission during the *Winds* phase. Our model results show during earlier *Winds* phase about 50% - 100% of total the ^{12}CO(1-0) line emission comes from the M7 cloud, but it decreases to less than 24% at the ^{12}CO(5-4) line, and to almost no contribution at $J > 5$. Our model M7 cloud has lower density than lower mass clouds (i.e. 3M3 - 3M6) and hence is less effective at exciting higher J transitions. The nonphysical small rise in T_{gas} at high A_V (see Fig. 5) has almost no effect on the CO (1-0) line flux. At around 1 Myr, the line intensity drops by three orders of magnitude because we have not included the gas swept up in the GMCs in the subsequent model of the shells (i.e. in the *post-SN* phase). These model line fluxes predicted for individual expanding shells can be used as a comparison with future observations, for example, the known expanding supershell centered around SNR 41.9 + 58 in M 82, in order to constrain the physical conditions of the gas and the age of individual shells.

In plot (b) of Fig. 8 the total line flux S_{CO} is calculated from all shells and their parent clouds in an ensemble with $3.1 \times 10^3 \leq M_{GMC} < 10^7$ $M_\odot$ (Shell + GMC Ensemble or SGE model). If multiple transitions CO data for individual expanding shells become available in the near future, models presented in plot (a) could be useful to constrain the burst age and gas mass in the shell, such as the supershell described in previous section. More than 80% of the ^{12}CO line emission arises from the massive shells (3M5 - M7) in the ensemble. The line SEDs have two distinct maxima with one near the $J = 6$ - 5 transition and another near

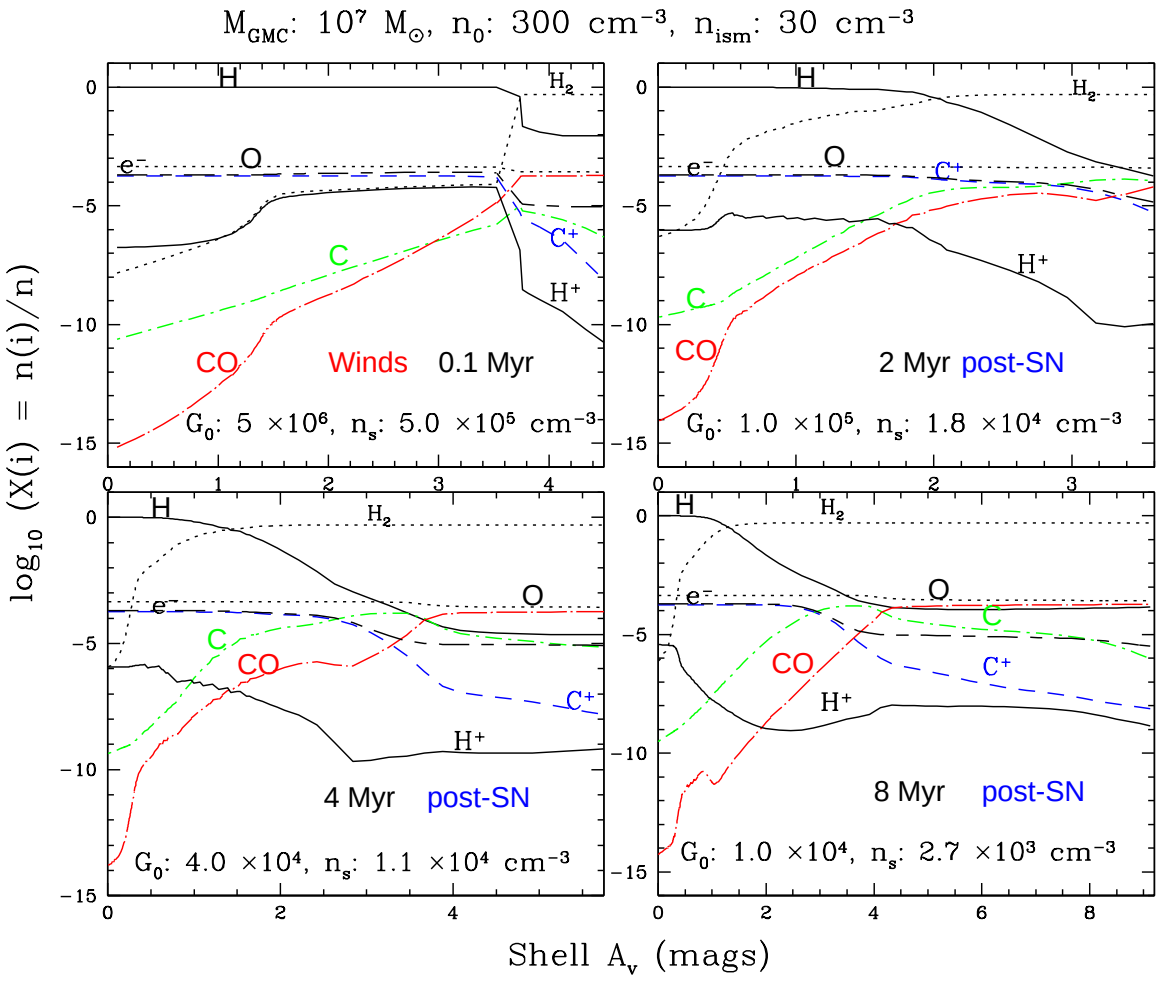

Fig. 6.— Plots of the time-dependent chemical abundances of the main species (H, H_2, H^+, e^-, C, C^+, O, and CO) relative to the total hydrogen density, as a function of visual extinction A_V for an M7 shell.

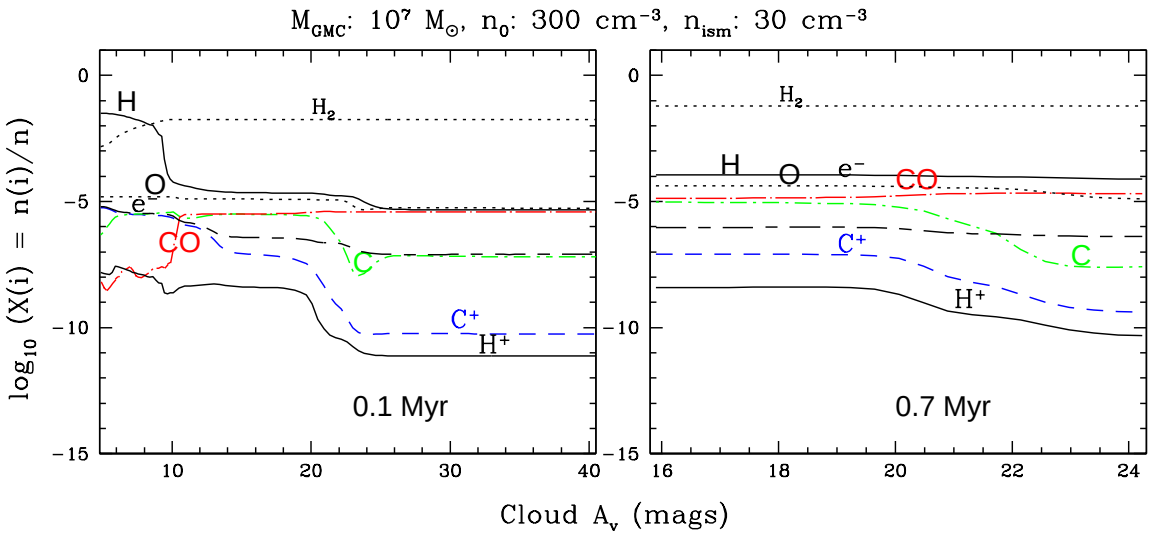

Fig. 7.— Plot of the time-dependent chemical abundances of the main species (H, H_2, H^+, e^-, C, C^+, O, and CO) relative to the total hydrogen density, as a function of visual extinction A_V for the most massive GMC M7 in the ensemble.

the $J = 3$ - 2 transition. The first maximum is associated with burst age between 0.3 and 7 Myr, and the second maximum is mainly associated with age older than 7 Myr. At age 0.2 Myr, the two maxima (4 - 3, 8 - 7) seen in the line SEDs are due to the sum of line emission of gas in the shells and parent clouds. It is clear that the CO excitation in the line SEDs varies with shell expansion or starburst ages. At ~ 1 ($\pm$ 0.2) Myr (*Winds* and *post-SN* phase transition), the S_{CO} is a few orders of magnitude lower than those for other ages. This is an artifact of the switch from *Winds* to *post-SN* phase, where the GMC mass swept up in the *Winds* phase is not carried forward into the *post-SN* phase, and the continuity equation (or mass conservation) is applied to the less dense ISM (i.e. $n_{ism} = 30$ cm^{-3}) instead of the GMC. Plot that shows the model line SEDs of ^{13}CO, HCN, HCO$^+$, and Table that calculates the fraction of ^{12}CO, HCN, and HCO$^+$ line emission from individual shells and their parent clouds are presented in Yao Thesis.

3.3.2. Atomic C, O, and C$^+$

The atomic forbidden transitions are the most important cooling lines arising in PDRs. The ratios of these lines and CO cooling lines can be used to derive the physical conditions in PDRs: for example, the incident FUV flux G_0, gas density n and temperature T_{gas}, as well as the ratio of G_0/n. By comparing these model line ratios with observations, we can constrain the physical properties of atomic gas within a detected region.

Upper left panels of Fig. 9 show the model line flux (in Jy km s^{-1}) for shell/GMC ensemble as a function of time for the [C I] 370μm line at 809.3 GHz and [C I] 609μm line at 492.1 GHz for the most massive shell/GMC and the shell ensemble. The [C I] 370μm transition has an excitation temperature of 63 K and a critical density of 3×10^3 cm^{-3}. Both values are higher than the [C I] 609μm transition (24 K and 5×10^2 cm^{-3}). The atomic line fluxes along with the molecular line fluxes that we presented here are for the template model of the star clusters and molecular H_2 clouds. The values for the actual masses for M 82 will be derived from a fit of the fluxes of this template model to the observed fluxes. The [C I] 370μm line flux emitted in the shells is generally higher than that in the [C I] 609μm line, whereas in the cooler less dense parent clouds seen during the *Winds* phase the [C I] 370μm to [C I] 609μm ratio is close to one (as seen in both plots (a) and (b)). The massive shells are the dominant source for the neutral carbon line emission in the *post-SN* phase. The discontinuity seen in the plots (near 1 Myr) is a result of switching phase from *Winds* to *post-SN* as explained previously in connection with molecular emission. Both line fluxes increases with time in the *post-SN* phase. The integrated fluxes of atomic lines predicted by our model generally increases with time, because more gas has been swept into the shells.

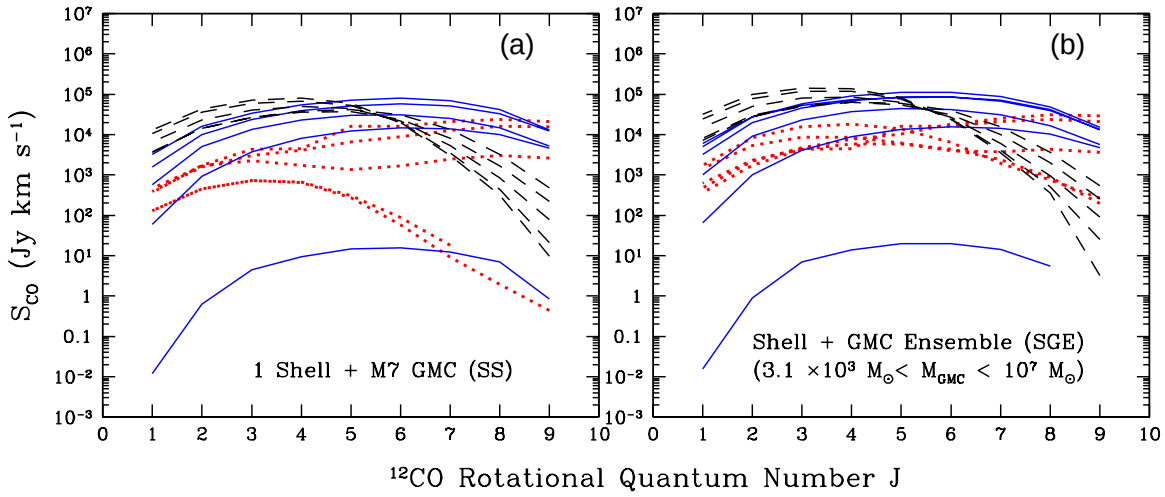

Fig. 8.— Plots of model ^{12}CO line SEDs for two different configurations. The *Winds* phase models are indicated by red dotted lines ($t \leq 0.7$ Myr), while the *post-SN* phase models are indicated by blue solid lines ($1 \leq t < 8$ Myr) and black dashed lines ($8 \leq t < 100$ Myr).

Upper right panels of Fig. 9 show the model line fluxes as a function of time for [O I] 63 μm line at 4744.8 GHz and [O I] 145 μm line at 2060.1 GHz. The intensity increases with time for both lines, and then levels off after 8 Myr due to a sub-thermal excitation, the critical densities of these two lines are above 10^5 cm^{-3}. The [O I] 63 μm line flux is clearly stronger than the [O I] 145 μm line throughout the entire starburst evolution. The [O I] 63 μm transition has a lower excitation temperature (228 K) than the [O I] 145 μm transition (326 K), and hence it is easier to be excited.

Lower left panels of Fig. 9 show the model line flux of [C II] 158μm line at 1900 GHz as a function of time. The [C II] 158μm line has an excitation temperature of 92 K and a critical density of 3×10^3 cm^{-3}. The flux of this line increases with time.

4. Understanding of Molecular Gas and Starburst Ages in M 82

In this section, we apply our evolving starburst models by comparisons to an expanding molecular supershell centered around the supernova remnant SNR 41.9 + 58 in the starburst galaxy M 82, and to the multiwavelength data of the central 1 kpc regions of M 82, in order to arrive at some conclusions about the nature of these two regions.

4.1. The Supershell Surrounding SNR 41.9 + 58

Observations have detected an expanding supershell centered around the bright SNR 41.9 + 58 in both molecular line and radio continuum (e.g. Weiss et al. 1999; Wills et al. 1999). This supershell has a diameter of $\sim$ 130 pc, an expansion velocity of $\sim$ 45 km s^{-1}, and a mass of $\sim 8 \times 10^6$ M$_\odot$. The kinetic energy of the observed supershell is estimated to be about 1.6×10^{53} ergs (Weiss et al. 1999). The kinematic evidence for the supershell appears most readily in the ^{13}CO(1 - 0) position-velocity (PV) plot (Neininger et al. 1998) as a depression on the west side of M 82, bounded by a feature emerging toward lower velocities and possibly blended with emission associated with gas following orbits in the bar potential. Neininger et al. (1998) conclude that the depression seen in the ^{13}CO(1-0) PV plot coincides with peaks in emission of [Ne II] and radio recombination lines, providing evidence that the void is populated by ionized gas inside the supershell. Seaquist et al. (2006) show that their PV plot reveals no depression in ^{12}CO $J = 6$ - 5 but instead find a region filled with ^{12}CO $J = 6$ - 5 emission that is not evident in the underlying ^{12}CO $J = 1$ - 0 map. Their line ratio PV map is consistent with the appearance of the channel maps, which show emission in the shell region extending over a very broad range in velocity. Seaquist

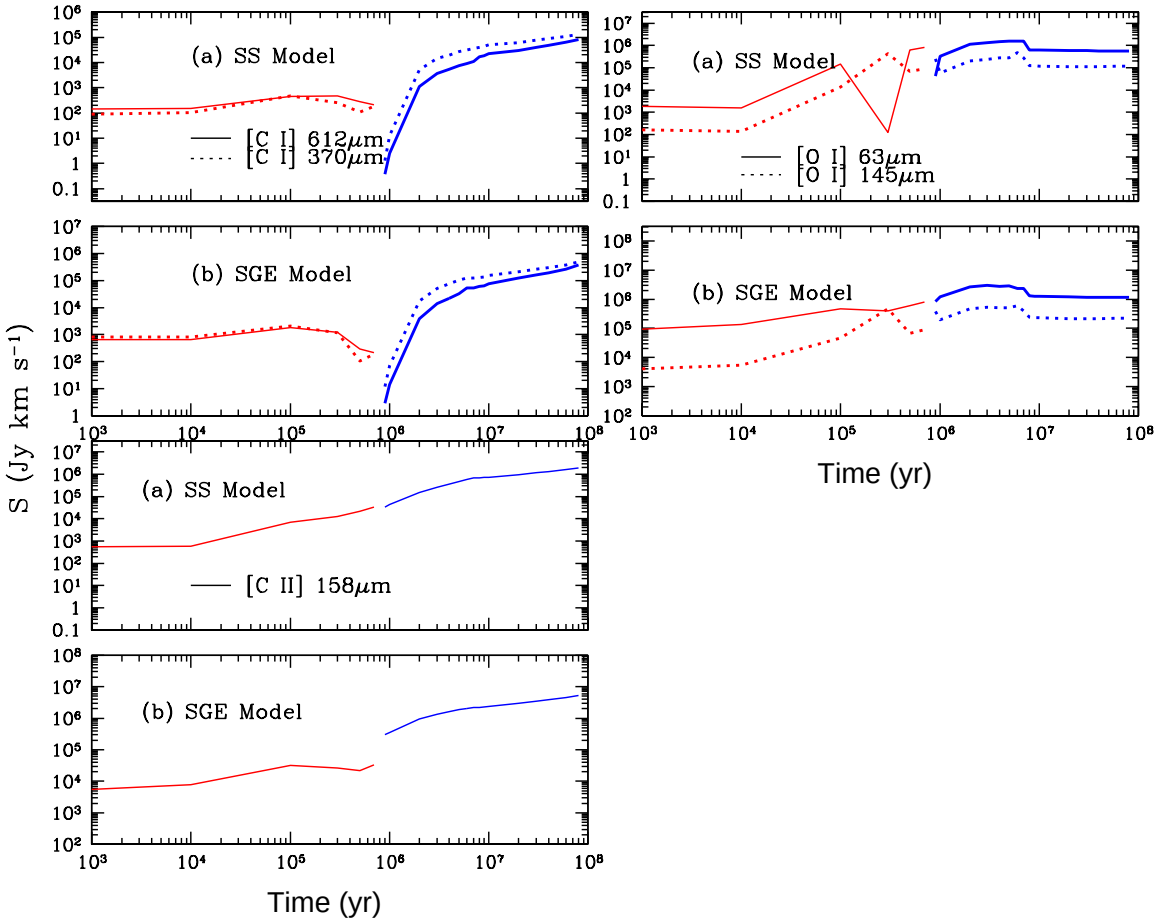

Fig. 9.— Plots of model atomic line fluxes (C, O, C^+) as a function of time. Upper left plots (a) and (b): the solid curves are the [C I] 609 μm lines, and the dashed curves are the [C I] 370 μm lines. Upper right plots (a) and (b): the solid curves are the O I] 63 μm lines, and the dashed curves are the [O I] 145 μm lines. Lower left plots (a) and (b): model [C II] 158μm line flux as a function of time. The red color indicates *Winds* model, and the blue color indicated *post-SN* model.

et al. (2006) conclude that the location of this supershell contains CO with higher than average excitation, together with the ionized gas. The cavity created by the supershell is not associated with prominent emission in higher density tracer such as HCN and HCO^+ in their low-excitation lines (Brouillet & Schilke 1993; Seaquist et al. 1998). This implies that the higher state of excitation may be due to higher kinetic temperature. Besides the known expanding supershell centered around SNR 41.9 + 58, there is evidence for other shells having sizes from several tens of parsecs to more than 1 kiloparsec, and kinetic energies between $\sim 10^{50}$ and 10^{55} ergs (e.g. Lo et al. 1987; García-Burillo et al. 2001; Wills et al. 2002; Bartel &Bietenholz 2005; Bayet et al. 2008).

The comparison of the kinetics of our single shell model with the observed supershell in M 82 is summarized in Table 3 of Paper I. Our model results and the observations agree remarkably well. In this paper, we investigate the state of excitation of the molecular gas in the supershell relative to that of the surrounding CO emitting gas in M 82, by comparing the predicted line ratios in the shell to those in the surrounding gas. For the surrounding gas we use line ratios computed for the bulk of the disk molecular gas based on our forthcoming analysis of fitting our model for a shell ensemble to the observed line ratios for the central 1 kpc (see § 4.2.2). Fig. 10 shows this for the line ratios of ^{12}CO high J transitions to the (1-0) transition (i.e. $I_{CO}/I_{CO(1-0)}$, I_{CO} in units of K km s^{-1}) for the model supershell. The jump in the ratios seen at $J = 3$ to 5 results from the addition of line emission of M7 shell to that of its parent cloud, where the GMC contributes 5 - 45% to the total line emission for $J \leq 4$, but less than 0.2% for $J > 4$. The plot shows clearly that our model for the supershell (red dashed curve) predicts that its line SED exhibits a higher level of excitation than the surrounding emission within M 82 (represented by the adjacent curve). Thus, one can expect some excess emission at high excitation transitions in the supershell after the underlying low excitation is subtracted out. Our model results are in qualitative agreement with the observational evidence for higher than average excitation emission in the supershell (e.g. Neininger et al. 1998; Seaquist et al. 2006). When higher quality and more extensive data on the excitation become available, our model predictions can be useful in interpreting the observations.

4.2. FIR/Sub-mm/mm Line Emission in The Central Region

Here we use the model components described in § 3 to produce a fit of our model line spectral energy distribution to the observations of molecular gas in the central 1 kpc region. The purpose is to determine whether it is possible to model the FIR/sub-mm/mm line emission in a massive star-forming galaxy, and whether there is a relation between the

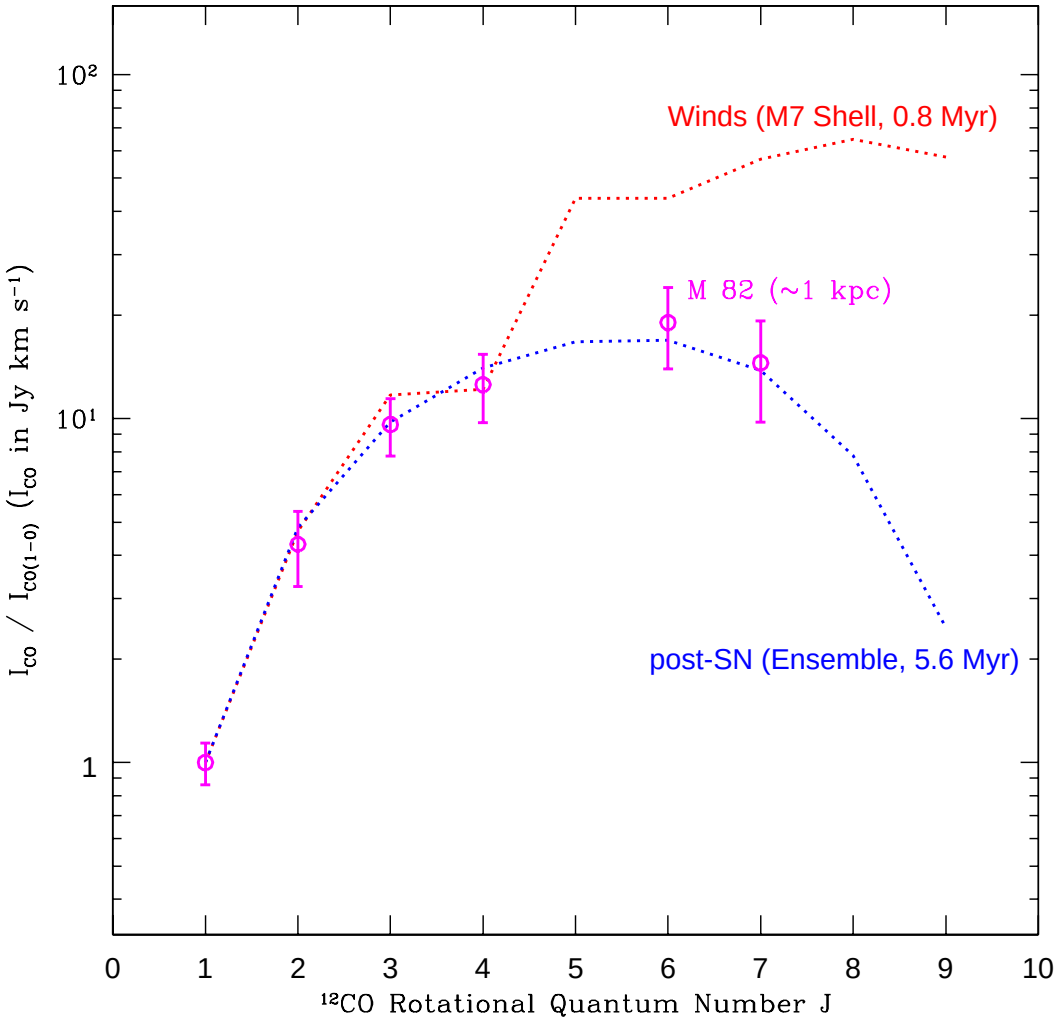

Fig. 10.— Plot of model line ratios of ^{12}CO high J transitions to the (1-0) transition (i.e. $I_{CO}/I_{CO(1-0)}$, I_{CO} in units of K km s^{-1}) as a function of rotational quantum number J for an expanding supershell (M7) at age 0.7 Myr (*Winds* phase, red dotted curve). For comparison, a similar plot is shown of the observed (magenta circles with errorbars) and modeled SED (blue dotted curve) of the central $\sim$ 1 kpc region of the disk of M 82 to represent the background disk emission with lower excitation. For details of the latter model fit, see § 4.2.2.

molecular gas properties and the age of the starburst (i.e. finding the *age indicator*), and to assess the overall impact of the starburst on the fine scale structure and physical conditions of the ISM in M 82.

We treat the entire central 1 kpc as an evolving starburst region, which can be modeled by following the evolution of an ensemble of expanding shells and clouds. Hence, different gas chemistry scenarios can be simultaneously at play in the center of this galaxy. However, our model does not attempt to reproduce or model the geometrical distribution of shells in an actual starburst system. In any event this distribution is unknown since the individual shells are not observed. The total line emission is assumed to be represented by the sum of the emission from all the shells in the model ensemble, which will then be used to compare with the observed data to estimate the stellar mass, the total H_2 mass, and the age of the associated starburst in the measured region.

4.2.1. Observational Data

The central concentration ($\sim$ 1 kpc) of molecular gas in M 82, which feeds the strong star formation activity, has been studied by many authors since the 1980s (e.g. Young & Scoville 1984; Wild et al. 1992; Gusten et al. 1993; Weiss et al. 1999; Mao et al. 2000; Petitpas & Wilson 2000; Weiss et al. 2001; Ward et al. 2003). Interesting results arise from these studies. For example, the observed CO line SED and line ratios can be reproduced by emission from low ($n(H_2) \approx 10^3$ cm^{-3}) and high ($n(H_2) \approx 10^{3.5-4.5}$ cm^{-3}, $T_{kin} \geq 40$ K) excitation gas components using a Large Velocity Gradient (LVG) method (Weiss et al. 2005, and references therein). The high excitation component, responsible for the excitation of levels beyond $J = 4$, arise from dense and warm gas, while the low excitation component is emitted by diffuse low density gas. The LVG method assumes a uniform abundance and velocity gradient across the modeling region, and no star formation history is considered as a cause for these conditions. It is this singular distinction which is the focus of this paper.

The excitation conditions of multiple transitions of dense gas tracers HCN and HCO^+ in M 82 have also been investigated, for example, by Seaquist & Frayer (2000). It was found from an LVG model, that both species are excited under a common set of conditions in star-forming regions where the $n(H_2)$ is near 10^5 cm^{-3}, $T_{kin} = 50$ K, and the abundances of HCN and HCO^+ are 2×10^{-8} and 1×10^{-8}, respectively (Seaquist & Frayer 2000). Molecular lines are commonly observed at $22''$ beam size, which covers about 680 pc of the center with a total H_2 mass of a few times 10^8 $M_\odot$ in M 82.

The atomic coolant, far-infrared lines in M 82, e.g. [C I] 370 μm, 609 μm, [O I] 63 μm,

146 μm, and [C II] 158 μm, have been studied by several groups (e.g. Stutzki et al. 1997; Colbert et al. 1999; Petitpas & Wilson 2001; Lord et al. 1996; Negishi et al. 2001, and references therein). As is the case for the molecular lines, the ratios of these cooling lines may be used to constrain physical parameters and possibly the age of the starburst. These ratios are sensitive to the physical and chemical conditions (density, temperature, and abundance), hence provide an opportunity to model the physical state of the neutral gas. In addition, unlike optical atomic line tracers, these FIR lines are relatively insensitive to extinction. A close examination of these lines emitted in M 82 may provide a template for future comparisons to infrared-bright, dust obscured starburst galaxies like M 82, including those at high-z.

In order to provide a useful indication on the starburst age(s), it is desirable to make comparisons with multiple transitions for various molecules and atoms. However, meaningful comparisons can be made only for regions where observations refer to the same beam size. The diagnostic tracers used in this paper are molecular ^{12}CO, its isotope ^{13}CO, HCN, HCO$^+$, and atomic C, O, and C$^+$. The low-J ^{12}CO lines are easily excited at relatively low densities and temperature, and are found essentially in every molecular gas cloud, and so they are good diagnostic tools for total molecular H_2 content, diffuse gas conditions, and star formation history. The less abundant ^{13}CO isotope has a much lower optical depth, and the line ratios between optically thin transitions in ^{13}CO are more reliable probes of the total gas content than ^{12}CO. The CO molecule is not considered a good tracer of dense and highly excited gas that is directly involved in starburst (i.e. earlier phase of star formation). However, molecular HCN and HCO$^+$ lines are more sensitive to dense gas (i.e. pre- or post-birth of stars) owing to their higher critical densities than CO. The atomic C, O, and C$^+$ fine structure lines are excellent probes of the PDRs in starburst regions, and their line ratios can be used for diagnosing the conditions of the associated FUV flux and gas density, as well as for indicating the ages of the later stages of starbursts.

In this paper, we use the observations of molecular and atomic gas in the central 1 kpc of M 82 described above. The molecular data for the center 1 kpc (along the major axis of the disk) are taken from Weiss et al. (2005). The molecular data for the center 680 pc are taken from Mao et al. (2000). The atomic data (Negishi et al. 2001, and references therein) to be used in our ratio-ratio diagram analysis, which are obtained from a larger area ($\sim$ 1.2 kpc) than for the molecular data. Note that the atomic C data are not included in our later ratio-ratio analysis, because the two [C I] line data correspond to different beam sizes (Stutzki et al. 1997). These molecular data will be used in comparisons with our models.

4.2.2. Model Fit to the ^{12}CO Line Spectral Energy Distribution

We consider first a model involving a single instantaneous starburst, and later consider whether extended starbursts could also provide an adequate fit.

Part I: Instantaneous Starburst Model

Our initial starburst model involves a single event in which all of the stars/clusters are formed simultaneously and instantaneously in the center of GMCs, associated with a unique age t and a star cluster mass M_* (corresponding to a GMC mass $M_{GMC} = 4M_*$ at the birth time). An instantaneous model, though physically unrealistic, is an acceptable representation of the SED if the duration of the star forming event is short compared to the age of the starburst. The intent is to derive these two parameters by fitting to the data. By extension, the total mass of H_2 swept-up in the ISM at any age is also determined.

The method used for fitting is the well-known numerical chi-squared (χ^2) procedure. The number of data points is six for the ^{12}CO data, and the number of free parameters (in this case) is two. The quantity S^J_{model} represents the corresponding model to be fitted, $S^J_{model}(f,\, t) = f\ S^J_{temp}\ (t)$, where $S^J_{temp}(t)$ is the model template line SED at age t, as given in Fig. 8 (see § 3), corresponding to a model template GMC mass M^{GMC}_{temp}, a model template cluster mass M^*_{temp}, and a model template swept-up mass by the shells M^{sh}_{temp}. The values for these parameters are $M^{GMC}_{temp} = 1.69 \times 10^7$ M$_\odot$, and $M^*_{temp} = 4.2 \times 10^6$ M$_\odot$. These initial masses correspond to the 127 clusters included in Table 1 (see § 2). The ratio of stellar cluster to GMC mass is 0.25 according to the assumed SFE. The adjustable dimensionless parameter f is introduced to control the amplitude of the model line SED (and hence the total cluster mass), and the age parameter t controls its shape and slope. These are simultaneously adjusted to provide the best fit corresponding to the minimum χ^2_ν. By assumption, the line fluxes $S^J_{temp}(t)$ are summed over the contributions of all clusters and GMCs, so that the best fit GMC mass M_{GMC}, cluster mass M_*, and the shell swept-up mass M_{sh} are determined from the corresponding best fit value of the parameter f by the relations,

$$M_{GMC} = f M^{GMC}_{temp}, \tag{3}$$

$$M_* = f M^*_{temp}, \tag{4}$$

$$M_{sh} = f M^{sh}_{temp} \tag{5}$$

We calculate χ^2_ν for a range of t and f. A minimum χ^2_ν value is obtained with a standard error estimation (i.e. the traditional likelihood method from using an inverse Hessian matrix

or covariance matrix). In the results there were found to be two minima with acceptable values of χ^2_ν(min), one for the *Winds* phase and the other for the *post-SN* phase. The chi-squared contour surrounding the minimum for the *post-SN* phase is shown in Fig. 11, where the contours are $\chi^2_\nu = \chi^2_\nu(\mathrm{min}) + i$ / (N - p), and i = 1, 2, 3, ..., corresponding to contour intervals of 1σ. The existence of a numerically acceptable solution for each phase signifies that there exist conditions in the molecular clouds of the *Winds* phase which are similar to those found in the compressed shells associated with the *post-SN* phase. However, only the *post-SN* phase solution is acceptable physically, since an age of 0.07 Myr derived for the *Winds* phase is implausibly small for a variety of reasons. For example, it is impossibly short compared to the dynamical time for the region (a few Myr) which would control the duration of the starburst. Such a small age might be barely plausible for an individual shell, but not for the molecular gas occupying this entire region.

The best fit line SEDs and ^{12}CO line SEDs at 4 and 7 Myr are shown superposed on the data in Fig. 12. The initial stellar mass and GMC mass are relatively small, but the impact on the surrounding ISM is significant. The total H_2 mass swept up by the shells is $\sim 2.0 \pm 0.1 \times 10^8$ $M_\odot$ at the best fit age of 5.6 Myr. This predicted value is in good agreement with the total gas mass within the central 1 kpc region obtained by other studies (a few 10^8 $M_\odot$) (e.g. Rieke et al. 1980; Mao et al. 2000). The model total stellar luminosity at this best fit is $\sim 1.4 \times 10^9$ $L_\odot$ using information from *Starburst99* based on our instantaneous starburst model.

In order to investigate how sensitive the results are to the assumed initial upper mass limit of the cluster spectrum (and corresponding GMC mass spectrum), we repeated the above analysis with revised upper mass limits of both 7.5×10^5 $M_\odot$ and 2.5×10^5 $M_\odot$ for the stellar spectrum, and corresponding GMC upper mass limits of 3×10^6 $M_\odot$ and 10^6 $M_\odot$ respectively. For the first case, we find $t = 5.0 \pm 0.4$ Myr, $f = 1.8 \pm 0.2$ with $\chi^2_\nu = 0.9$, and for the second case an unacceptable fit with a $\chi^2_\nu = 33$. Thus, a comparable solution may be found with a choice of a slightly lower upper mass cutoff, but no acceptable solutions are found with values reduced by a factor of 10 or more in the upper cutoff of the cluster mass spectrum. We conclude that the model can provide acceptable fits to the data only if the dominant initiating starburst clusters are massive, at least 5×10^5 $M_\odot$.

Our models show that the H_2 density of the shells at the best fitted age 5.6 Myr is between 10^3 and 10^4 cm^{-3}, and the gas temperature is $\sim$ 50 - 100 K. These values are comparable with the two-component LVG predictions (Weiss et al. 2005). The evolution of CO abundance as a function of A_V is illustrated in Fig. 6. The CO abundances in massive shells (M6 - M7) are above 10^{-5} with respect to the total H density, providing most of the CO emission.

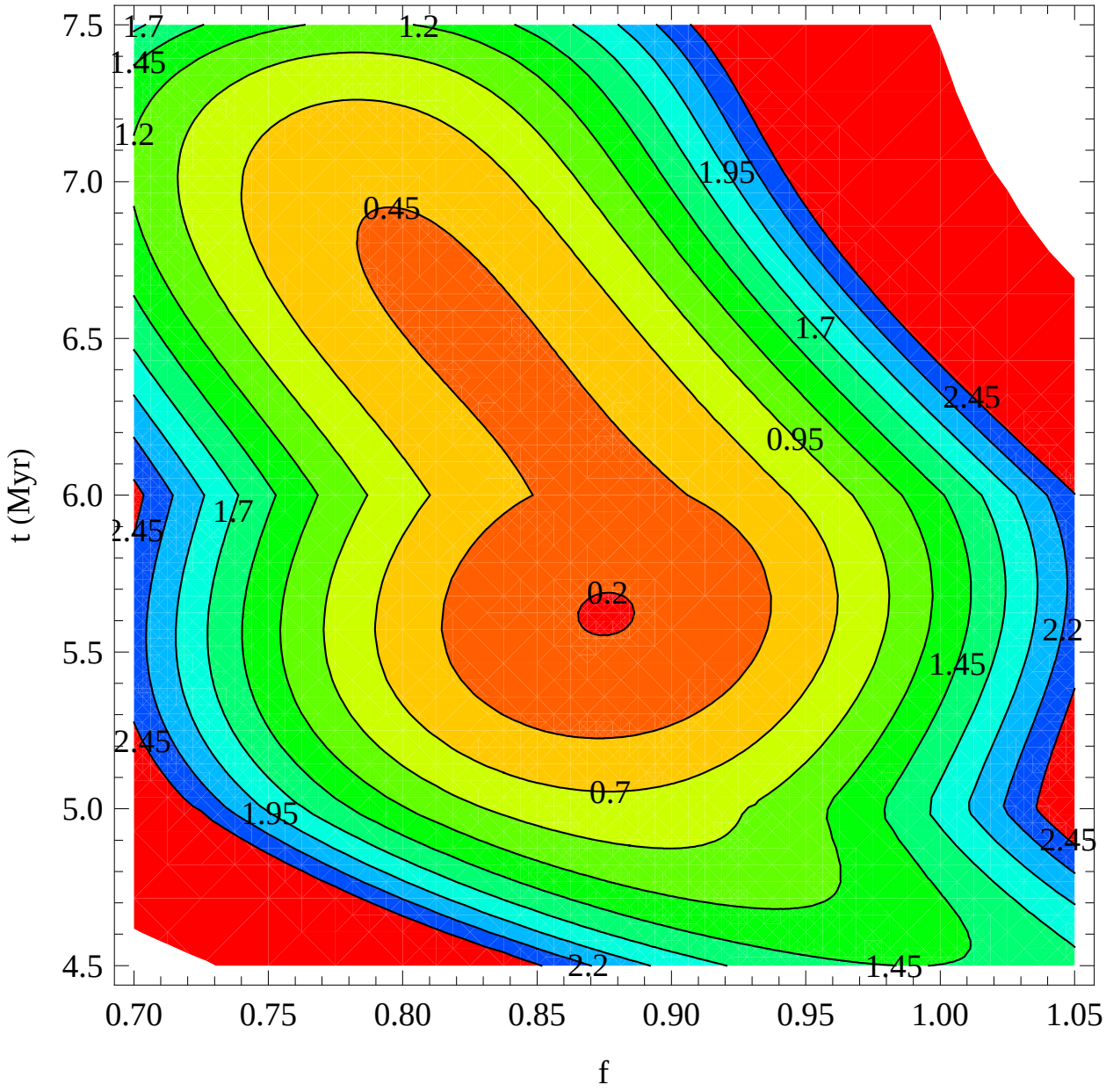

Fig. 11.— A contour plot of χ^2 values as a function of mass coefficient f and burst age t at the *post-SN* phase.

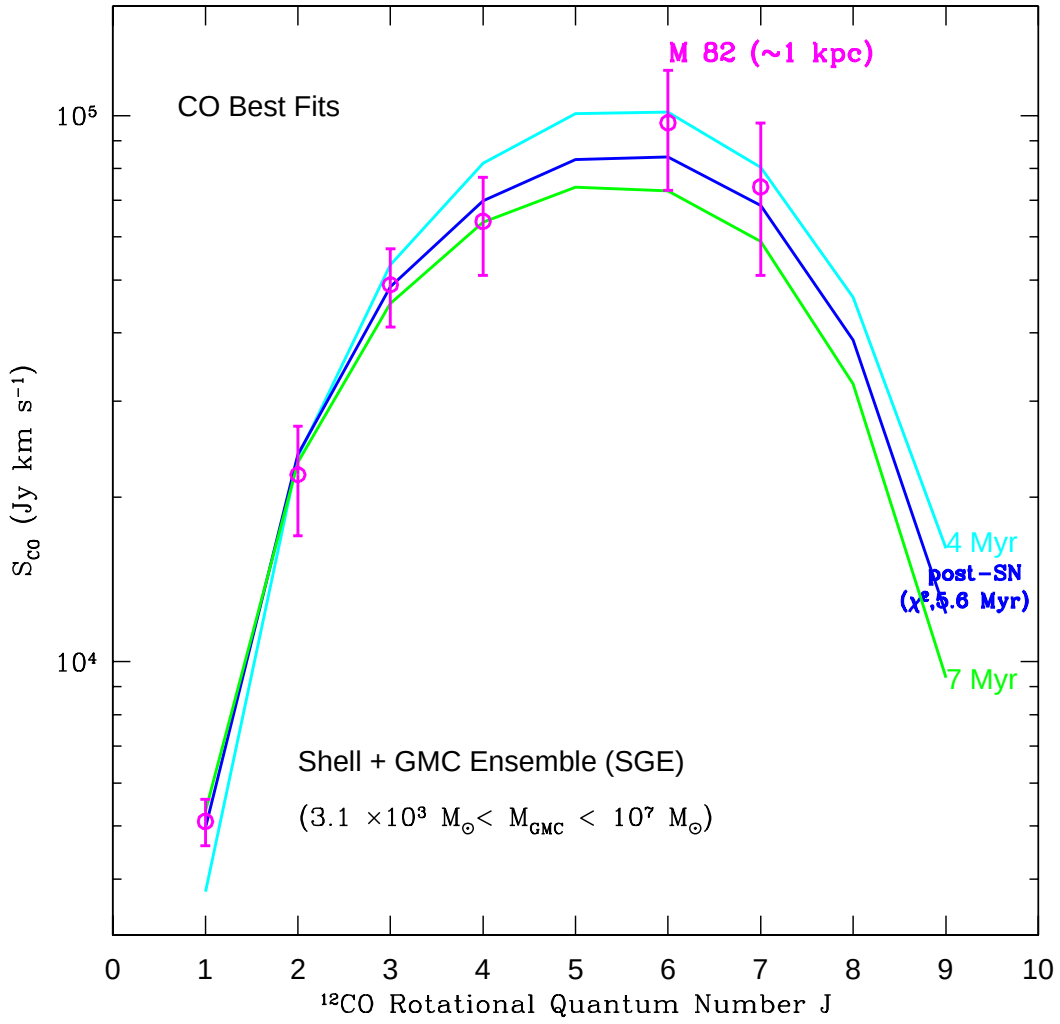

Fig. 12.— A χ^2 fit of an instantaneous starburst model to the ^{12}CO line SED for the central 1 kpc disk region of M 82. The blue curve is the best age at 5.6 Myr for the *post-SN* phase, the cyan curve is the line SED at 4 Myr, the green curve is the line SED at 7 Myr, and the observed data are indicated by magenta open circles with error bars (Weiss et al. 2005).

Part II: Extended Starburst Model

The foregoing discussion and results assume an instantaneous starburst with the result that our CO best fit model has an age of 5.6 Myr. The question naturally arises whether a model with a period of more continuous star formation would also provide a satisfactory solution. One can anticipate that the answer might be yes, if the best fit line SED were to be roughly equally represented by the SED of an outburst at one epoch, or an average SED over some time period roughly centered on, and symmetrically distributed about this epoch. Fortunately, it is straight forward to test this hypothesis since the SED for a smoothly varying star formation model may be constructed from a superposition of instantaneous bursts at different times.

We are thus led to consider the extreme case of a uniform star formation rate (or SFR) occurring between an epoch 10 Myr ago and the present time. This starting point of the event may be considered appropriate because the most massive shells from even earlier epochs would now be large enough to exceed the thickness of the nuclear disk and thus their emission would begin to fall outside the region modeled. Fortuitously, this period is also almost symmetrically distributed about the epoch for the best fit instantaneous model.

We do not discuss the procedure in detail here, since the analysis proceeds as before, but with only one parameter, namely the star formation rate over the past 10 Myr. The SED employed is then an integral of the CO line SED profiles over a time period of 10 Myr. The result is that an acceptable fit (minimum $\chi^2_\nu = 0.78$) can be found for a continuous SFR $= 0.5 \pm 0.05$ $M_\odot$ yr^{-1}. The total stellar mass produced during this period is $(5.0 \pm 0.5) \times 10^6$ $M_\odot$, which is, not surprisingly, close to the total mass (i.e. 4.3×10^6 $M_\odot$) required for the single epoch model. The conclusion is that a uniform SFR over the past 10 Myr also produces a satisfactory fit to the ^{12}CO data. In addition, it may be plausibly inferred that a variety of star formation histories would work, provided the SFR rate profile is more or less symmetrically distributed about the epoch of 5.6 Myr.

The implication of this result is that in terms of the agreement between the model and the data, the star formation need not be instantaneous, or even sharply peaked at 5.6 Myr. However this epoch nevertheless represents a unique point of time associated with the history of star formation in M 82 since it would emerge from various representations of the star formation profile. If there were an instantaneous starburst in M 82, then its age is approximately 5 - 6 Myr (plus or minus a factor of about 2). However, the SED is also consistent with continuous star formation rate of 0.5 $M_\odot$ yr^{-1} over at least the last 10 Myr. The factor of 2 is our estimate of the uncertainties introduced by the uncertain density of the ambient interstellar medium in the model, as well as our assumption that the shells do not stall.

4.2.3. Molecular and Atomic Line Ratio Diagrams

The line intensity/flux ratio-ratio diagram can be another diagnostic tool for studying the gas excitation conditions and properties, as well as their relations to starburst evolution, especially when there are not enough data points available for the type of model fitting discussed in the previous section. Since the line ratio is independent of the total gas mass in the measured region, the ratio-ratio diagram cannot be used to provide an estimate of the total gas mass directly. However, once the age t is obtained, we can scale the template line flux spectrum to the flux observed, and calculate the model value for the swept-up H_2 mass.

^{12}CO and Its Isotope ^{13}CO

Fig. 13 illustrates the ratio-ratio diagrams for different transitions involving ^{12}CO and ^{13}CO predicted by our model (*post-SN*), and a comparison with the observations. The observed data refer to the center of M 82 with a beam-width of $22''$ (see Table 1 in Mao et al. 2000). All line brightnesses are compared in units of Jy km s^{-1}. The isotope abundance ratio [^{12}CO]/[^{13}CO] of 55 is adopted for the ensemble modeling. In the plots, we include the systematic uncertainties (31% for ^{12}CO(7-6), 20% for ^{12}CO(4-3), 16% for ^{12}CO(3-2), 23% for ^{12}CO(2-1), 10% for ^{12}CO(1-0)) into the line ratio error estimations (i.e. sizes of error bars). In plot (a) the model ratios of ^{12}CO(7-6)/(4-3) versus (2-1)/(1-0) match nicely (as expected) with the observations at age 5 - 6 Myr for the center 680 pc region. It is similar to the age derived from the chi-squared fit to the ^{12}CO line SED in the center 1 kpc region (Weiss et al. 2005) even though the angular size of the region is different. This is expected, since $\sim$ 65 - 80% of the ^{12}CO emission from the inner 1 kpc disk originates from the central 680 pc starburst regions. Plots (b) and (c) show a poor match between our model line ratios of ^{13}CO(3-2)/(2-1) versus (2-1)/(1-0) and ^{12}CO(2-1)/^{13}CO(2-1) versus ^{12}CO(1-0)/^{13}CO(1-0) (blue-dashed curves) and the observed data. The closest match within the observed uncertainties is 7 - 8 Myr for plot (b), 5 - 6 Myr for plot (c), where the latter is in a fair agreement with ^{12}CO best fitted age.

Our model fails to produce the right ratios for lines involving ^{13}CO. If the choice of the isotope abundance ratio is to be considered as the reason for such poor fit, adopting a different isotope abundance ratio (55 is used in this paper) can affect the result in plot (c) but not that in plot (b). Mao et al. (2000) indicated that their ^{13}CO(2-1) values should be considered with caution, due to uncertainty of convolving a smaller beam ($13''$) to a larger beam size ($22''$). If we assume that the best match age for plot (b) and (c) should be between 5 and 6 Myr, and if we assume that an erroneous value for the ^{13}CO(2-1) model flux is the reason for lower ratios seen in plot (b) and (c), we estimate that this value is underestimated

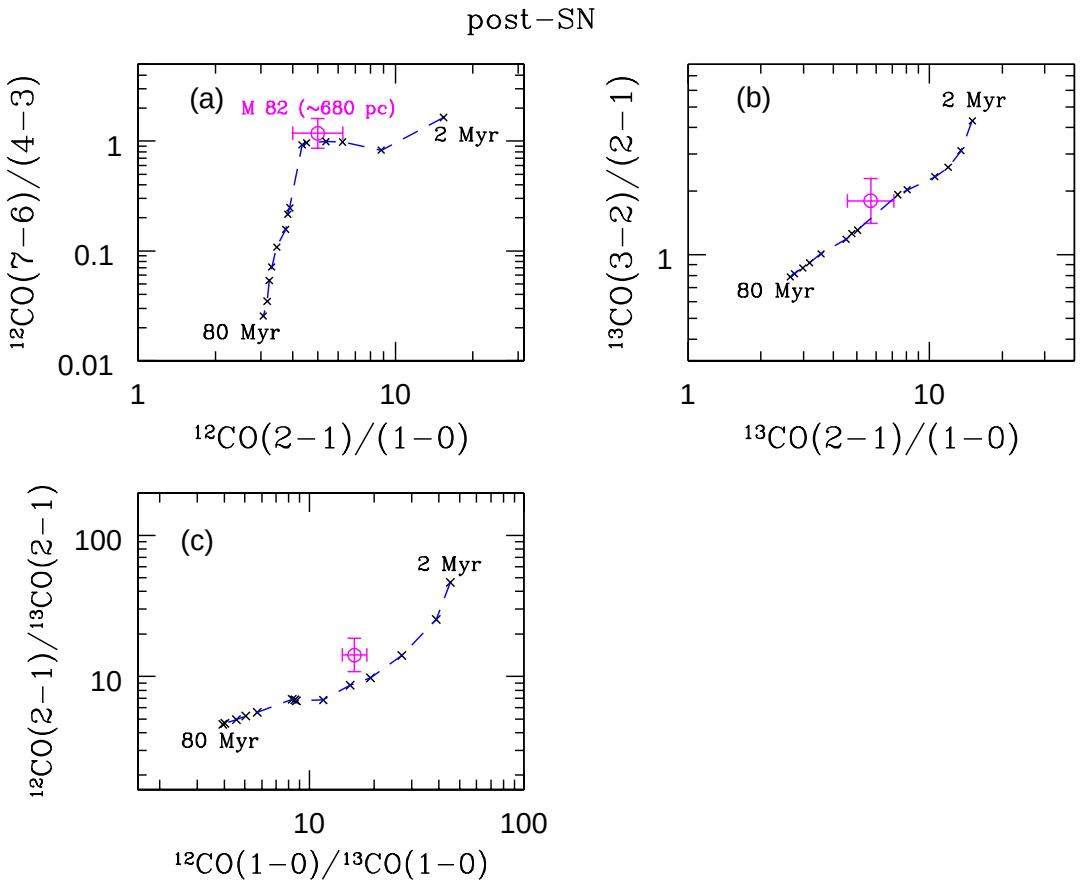

Fig. 13.— The ratio-ratio diagrams of molecular ^{12}CO and ^{13}CO line intensities (in units of Jy km s^{-1}). Model results for a shell ensemble are indicated by the crosses connected with blue dashed lines. The age sequence is 2, 3, 4, 5, 6, 7, 8, 9, 10, 20, 30, 40, 60, and 80 Myr. The magenta filled circles with error bars are the observed data (22″ resolution data for the center of M 82 from Table 1 of Mao et al. 2000; the errors include systematic uncertainties).

by a factor of 1.5. Another factor that contributes to the poor match between our model results and the data is that the line ratios involving ^{13}CO may be particularly sensitive to optical depth if the intensities are not optically thick.

We also investigated the effect of reducing the upper mass limit to the GMC mass spectrum as was done for the ^{12}CO model, and found that changing the upper mass limit to the GMC mass spectrum has no effect in resolving this problem.

Atomic O and C$^+$

Fig. 14 shows the model ratio-ratio diagram for [O I]63μm/[C II]158μm versus [O I]63μm/[O I]145μm, and a comparison with the observations of these atomic lines from the central 1.2 kpc region in M 82 (Negishi et al. 2001). All line fluxes are compared in units of W m^{-2}. The model [C II]158μm line flux may be underestimated, since we ignore the line emission that arises from the H II region. A good match between our model and the observation is obtained with age $t \sim 10$ Myr. The age predicted from atomic data is older than the age ($\sim$ 5 - 6 Myr) derived from our ^{12}CO line SED analysis. This may be because the atomic line data are based on a $80^{''} \times 80''$ beam area whereas the ^{12}CO line data pertain only to the $60^{''} \times 18^{''}$ beam area. We suggest that these two ages may be a result of sampling different regions. More discussion of this possibility will be given in § 4.3.2.

The ranges of gas conditions for the model shells at 10 Myr are $G_0 \sim 350$ - 1.4×10^4, $n(\mathrm{H_2}) \sim 10^2$ - 2.4×10^3 cm^{-3}, and $T_{gas} > 20$ K. The gas conditions derived from our atomic models for this sampling region are comparable with the study by Colbert et. al. (1999) (G_0 = 630, $n = 2.0 \times 10^3$ cm^{-3}), but the age is greater than that (3 - 5 Myr) derived by Colbert et al..

The total molecular gas swept up into shells cannot be obtained directly from the ratio-ratio diagram. However we can obtain this from the ratio of observed [O I]63 μm line flux to the model template [O I]63 μm flux at age 10 Myr, i.e. $f = S_{obs}$ / $S^{temp}_{model} = 0.84$, where $S_{obs} = 169 \times 10^{-15}$ W m^{-2} and $S^{temp}_{model} = 202 \times 10^{-15}$ W m^{-2}. We compute the total $\mathrm{H_2}$ gas in the measured $80^{''}$ region by multiplying $f = 0.84$ by the model template $\mathrm{H_2}$ mass M^{temp}_{model}. Hence, the result is $M(\mathrm{H_2})$ at age 10 Myr is $\sim 3.4 \times 10^8$ M$_\odot$.

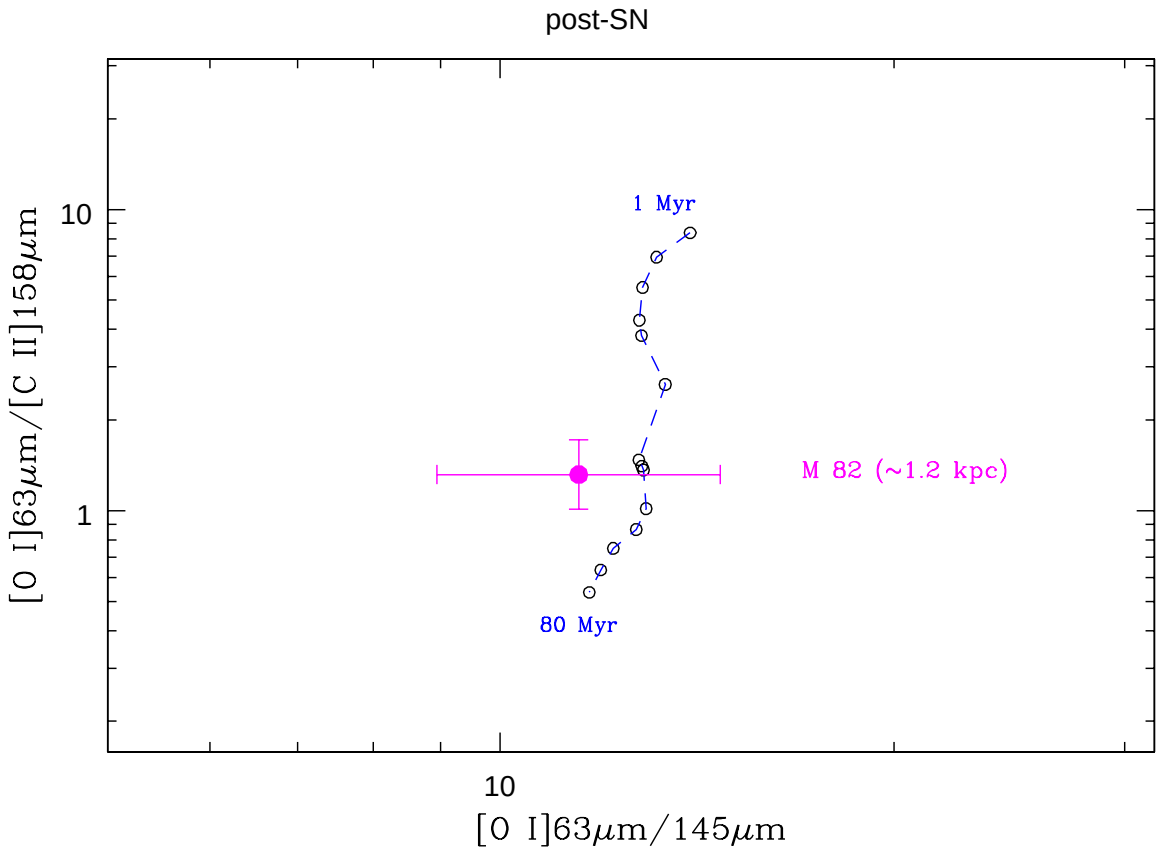

Fig. 14.— The ratio-ratio diagram of atomic fine structure line fluxes (in units of W m^{-2}). The models are indicated by open circles connected with a blue-dashed curve for *post-SN* phase. The age sequence is 1, 2, 3, 4, 5, 7, 8, 9, 10, 20, 30, 40, 60, and 80 Myr for the *post-SN* phase. The filled circle with error bars show the observed data for the center 1.2 kpc of M 82 (Negishi et al. 2001).

4.3. Discussion

4.3.1. An Expanding Supershell Associated with SNR 41.9+58

The very good agreement between our supershell kinematic model and the observations is consistent with the hypothesis that this expanding supershell is created by strong mechanical winds from a young star cluster with a total mass of about 2.5×10^6 $M_\odot$ which formed at its center about 0.8 Myr ago. This agreement also suggests that the set of models we have put forward in this paper may be used to interpret other shells in M 82 or shells in other starburst galaxies. Although like any other model, the result depends to some degree on the set of initial conditions and assumptions that we selected for our models. The reliability of the age and mass for this supershell derived from our kinematic study needs to be further examined in near future when high resolution maps of multiple transitions of CO emission in this shell are available to compare with our model. Meanwhile we relate our model CO line ratio SED (i.e. $I_{CO}/I_{CO(1-0)}$ as a function of J) for the SNR 41.9 + 58 (i.e. M7) supershell at age 0.8 Myr to the corresponding line SED for the surrounding gas in the inner 1 kpc starburst region of M 82. We show that the emission in the M7 supershell exhibits a higher degree of excitation than the surrounding emission (see Fig. 10).

There are a number of issues arising from the supershell study. They are as follows: (1) it is interesting to ask whether our results are consistent with a possible physical association between the supershell and the bright SNR 41.9 + 58 near its center. If the bright SNR were within or near the SSC, there may not be sufficient gas remaining to form an SNR after the action of the winds from the cluster; and (2) the SSC responsible for the formation of the supershell might also have provided the stellar mass for the several hundred solar mass black hole detected by Chandra X-ray observations near its center (e.g. Dewangan et al. 2006). Theories for the formation of this black hole include the collapse of a *hyperstar* formed by the coalescence of many normal stars, or the direct merger of stellar mass black holes (e.g. Kawakatu & Umemura 2005). The SSC is adequately endowed with sufficient mass since there would have been 1,700 O stars, each with mass greater than or equal to about 40 $M_\odot$ (Yao et al. 2006).

4.3.2. Central Starburst Region

Age of Recent Starburst and Star Formation History

Given the complexity of M 82, a full understanding of star formation epochs requires various diagnostic tools to trace different ISM components in starburst regions. Especially

since both optical and near- to mid-infrared emissions are subject to higher extinction in dusty media, the selection of SSCs may be biased toward either younger or older age as mentioned before. Since the ISM is nearly transparent to FIR/sub-mm/mm emission, the analysis in this paper, employing atoms and molecules emitting in this range, forms a useful complementary investigation to those already mentioned. Using our evolving starburst model for neutral gas media, we have been able to probe the recent star formation history of M 82 throughout the entire volume of the central starburst region.

The starburst ages derived from optical and infrared spectra are 5 - 6 Myr, 10 - 25 Myr, and 30 - 100 Myr. The age derived from our analysis of CO line SEDs and ratio-ratio diagrams is 5 - 6 Myr for the central 1 kpc × 280 pc rectangular regions; although the region used is 1 kpc, about 70% is concentrated toward more central regions ($\sim$ 350 pc). The age derived from our atomic data is slightly older, i.e. 10 Myr for a larger area ($\sim$ 1.2 kpc). We suggest that these two ages may be a result of sampling different regions as mentioned earlier. It is unclear from our analysis whether these two ages refer to the same period of star forming activity or to two spatially separated independent bursts. A more sophisticated model and more data are needed to clarify the picture.

The burst ages derived from our model are similar to the results found in the aforementioned studies by Förster-Schreiber et al. (2003) and Efstathiou et al. (2000). However, for the atomic data there is a discrepancy between our result (10 Myr) and the study by Colbert et al. (1999) (3 - 5 Myr) using a similar set of data (by Negishi et al. 2001). Nevertheless, our derived gas conditions for the shells at 10 Myr ($G_0 \sim 350$ - 1.4×10^4, $n(\mathrm{H_2}) \sim 10^2$ - 2.4×10^3 cm^{-3}, and $T_{gas} > 20$ K) are similar to those derived by Colbert et al.. The age discrepancy may be caused by differences in the choice of models, for example, Colbert et al. used the CLOUDY PDR model to compute the atomic line fluxes, while we use the UCL_PDR model and a non-LTE radiative transfer model to compute the line fluxes.

Molecular Gas Properties

Our evolving shell models yield familiar values for the gas density, temperature, and structure scales compared to those measured in the center of M 82 (e.g. Lynds & Sandage 1963; Rieu et al. 1989; Stutzki et al. 1997; Seaquist & Frayer 2000; Mao et al. 2000; Negishi et al. 2001; Ward et al. 2003). For an extended starburst scenario ($SFR = 0.5 \pm 0.05$ M$_\odot$ yr^{-1} as discussed in § 4.2.2), the shell densities are in the range 10^2 - 10^6 cm^{-3}, and the gas temperatures are in the range 20 K to 1000 K across the shell for various shells. The total H_2 mass swept up by the shells within the inner 1 kpc ($\sim 2.0 \pm 0.1 \times 10^8$ M$_\odot$) and 1.2 kpc ($\sim 3.4 \pm 0.3 \times 10^8$ M$_\odot$) detection regions are compatible with those derived from the CO luminosity using the CO-to-H_2 conversion factor (Wild et al. 1992; Mao et al. 2000; Walter et al. 2002).

It is also comparable with the total ambient gas mass in our model. Hence, the picture suggested is that of a *porous* neutral ISM in the central star-forming region of M 82, a product of evolving shells. In reality, many or most shells are probably in the form of fragments, small cloud clumps, sheets, or partial and full circular arcs (e.g. Lo et al. 1987; Yao et al. 2006, and references therein).

Molecular Ring Formation Mechanism

Although different stages of starburst evolution are applicable to different central regions of M 82, the shell sizes and the physical conditions of the gas within the rings (diameter $\sim$ 300 - 600 pc) predicted by our model are similar to what is expected from models involving expanding shells from a central starburst such as those proposed by Carlstrom & Kronberg (1991). Their hypothesis is that molecular rings in M 82 are a result of compressed gas in a starburst region. This hypothesis is supported by the observations of the geometrical structure of the CO line emission and continuum emission, as well as the discovery of supershells that have not yet had time to break out of the galactic plane. However, the conclusion drawn from the shell size and average gas conditions in the inner 1 kpc region is only suggestive, since our model does not handle the physical distribution of molecular gas in the center of M 82. It is also important to realize that the foregoing interpretation of the lobes as a ring is not unique. A number of authors have argued that the molecular rings are a product of Linblad resonance instabilities associated with the gravitational effects of the bar (e.g. Shen & Lo 1996; Wills et al. 2000).

4.3.3. Limitations of Our Model and Their Impacts

We have demonstrated that the kinematic and FIR/sub-mm/mm emission properties of individual expanding shells and star-forming regions in a starburst galaxy like M 82 can be understood by following the evolution of individual massive super star clusters or an ensemble of such clusters surrounded by compressed shells and GMCs. It is an important piece of complementary work to the existing optical and infrared studies, and it helps us to obtain a more complete and or accurate picture of star formation episodes in the center of M 82.

However, our model also has a number of caveats, limitations, and potential sources of systematic error. Here is the important list:

(1) We have neglected throughout the effects of the ambient pressure in slowing down and perhaps stalling the shells. This applies to both *Winds* and *post-SN* phases. We recall

that the shells will stall when their expansion velocities decrease sufficiently that they are approximately equivalent to the sound speed $(P/\rho)^{\frac{1}{2}}$ of the external medium. To estimate the effects of this pressure, we can thus compute the sound speed associated with estimates of the pressure and compare this with the shell speeds. We compute the total pressure P_{cloud} inside the cloud, assuming it is in virial equilibrium from the following equations (McCray & Kafatos 1987),

$$P_{cloud} = P_{ext} + P_{intern}, \quad (6)$$

$$P_{ext} = 2n_0kT, \quad (7)$$

$$P_{intern} = 0.5G\Sigma^2 \quad (8)$$

where P_{exter} is the external pressure, P_{intern} is the internal pressure, n_0 is the cloud H_2 density, k is the Boltzmann constant (1.38×10^{-16} erg K^{-1}), G is the gravitational constant (6.67×10^{-8} cm^3 g^{-1} s^{-2}), and $\Sigma = M_{GMC}$ / (π R^2_{GMC}). The sound speed in a GMC can be calculated from the equation,

$$c_{cloud} = \Big(\frac{P_{cloud}}{\rho_{cloud}}\Big)^{\frac{1}{2}} \quad (9)$$

We obtain a sound speed of $c_{cloud} = 19$ km s^{-1} in a M7 cloud ($n(H_2) = 300$ cm^{-3}, M_{GMC} = 10^7 $M_\odot$, and $R_{GMC} = 47$ pc), assuming $P_{ext}/k = 10^7$ K cm^{-3} in starburst regions of M 82 (Silich et al. 2007), where k is the Boltzmann constant. We can further combine Equations (16) through (19) with the cloud relations Equations (7) and (8) to furthermore yield the sound speed in any given GMC,

$$c_{cloud} = 19\ kms^{-1}\Big(\frac{M_{GMC}}{10^7 M_\odot}\Big)^{\frac{1}{4}} \quad (10)$$

For the external ambient medium, we use the aforementioned external pressure to obtain the sound speed for the ISM ($n_{ism} = 30$ cm^{-3}),

$$c_{ism} = 40\ kms^{-1} \quad (11)$$

The comparison between sound speeds inside the clouds (Equation (20)) and shell expansion velocities for the *Winds* phase indicates that shells from cloud masses above 10^5 $M_\odot$ would not be trapped, and those equal or below this mass would be stalled if the effects of cloud pressure were included.

We also compare the sound speeds in the ISM (40 km s^{-1}) with shell expansion velocities for the *post-SN* phase. For example, for the shells associated with the three most massive GMCs, namely M7, 3M6, and M6 in our model ensemble, the shells have radii of 220, 180, and 130 pc at the best fit age 5.6 Myr without ambient ISM pressure, respectively. But the stall radii and ages for these three shells are 112 pc at 2 Myr, 70 pc at 1.2 Myr, and 42 pc at 0.8 Myr, respectively. Thus, without the inclusion of the effects of pressure it may be said that the shell radii at the time of observation are probably overestimated by more than a factor of two compared to the stall values when pressure is included. Since the swept-up mass by the shell is proportional to the R_s^3, an overestimate by a factor of two in shell radius would yield a factor of eight in the total swept-up mass for a given GMC/SC mass. This may help to understand the shortfall in IR luminosity predicted by our starburst model (see point (3) for detailed discussion).

Another issue worth mentioning is that the confining pressure will vary greatly with location in the galaxy, especially between the center and the edges of the disk where some of the observed supershells are located. For example, as we mentioned earlier in this chapter, observations have detected an expanding supershell centered around the bright SNR 41.9 + 58 in both molecular line and radio continuum (e.g. Weiss et al. 1999; Wills et al. 1999). This supershell has a diameter of $\sim$ 130 pc, an expansion velocity of $\sim$ 45 km s^{-1}, and a mass of $\sim 8 \times 10^6$ $M_\odot$. If $P_{ext}/k = 10^7$ K cm^{-3} were the relevant external pressure in this case, then this shell will stall soon. However, the pressure may well be lower than the above value in this region, since part of the shell is seen outside the disk. Other expanding shells (incomplete arclike shapes) with velocities possibly as low as 10 to 15 km s^{-1} with radii $\sim$ 200 pc are also observed in the central region (Lo et al. 1987), suggesting a sound speed less than the 40 km s^{-1} figure used above.

(2) Observations of nearby bubbles in our own Galaxy and in the Magellanic Clouds indicate that the simple adiabatic bubble/shell theory (Weaver er al. 1977; McCray & Kafatos 1987) coupled with the mechanical luminosities calculated by *Starburst99* for this paper leads to significant overestimates of the bubble pressure and hence the shell radius (e.g. Oey & García-Segura 2004, and references therein). Either the wind power is lower or some hot bubble gas escapes from the bubble interior. In addition, Dopita et al. (2005) argued that the conventional bubble/shell dynamical model may overestimate the winds and supernova mechanical power. Another argument is that gravitational instability may induce new star formation inside the shells. If such effects were present, they would have an impact on the estimate of the total stellar mass and luminosity in our model, as described in more detail in point (3).

(3) The bolometric luminosity for the best fit cluster mass of 3.7×10^6 $M_\odot$ and best fit

age of 5.6 Myr is 1.5×10^9 $L_\odot$ (based on *Starburst99* model). The observed IR luminosity of M 82 disk is about 3.0×10^{10} $L_\odot$. Since the bolometric luminosity should be an upper bound to the IR luminosity from the same stars, the shortfall in the model luminosity is at least a factor of 20. This shortfall is similar to that (also about a factor of 20) between the star formation rate derived from our continuous star formation model (~ 0.5 $M_\odot$ yr^{-1}), and the measured star formation rate $\sim$ 5 - 10 $M_\odot$ yr^{-1} for the center of M 82 (e.g. de Grijs et al. 2001; Lipscy & Pl avchan 2004). Hence, the stellar cluster mass needed according to the model to produce the observed CO luminosity is not sufficient to account for all of the stellar luminosity or young stellar mass in M 82.

There are several reasons that our shell ensemble model may have overestimated the swept-up gas mass and the line emission for a given cluster mass, or equivalently underestimated the stellar mass and luminosity required for a given swept-up gas mass. Points (1) and (2) above show that our model itself may be fundamentally optimistic in its impact on the ISM, i.e. the model shells may be too big for the stellar mass which generates them, thus leading to an overestimate in the swept-up shell masses and CO luminosity per unit stellar mass. The radii of the shells are larger than they would be in a more realistic model where the pressure of the ISM is included and where the effects of lower mechanical luminosity and leakage of bubble gas are included. These might be major effects and they both act in the same direction. If the shells at the best fit age are smaller, then we simply need more of them to build up the H_2 mass sufficient to explain the observed CO flux. In particular, if the shells were to stall early at radii about half that in our model, then a model which includes this effect would require about eight times the cluster mass for the shell ensemble. This factor already accounts for much of the missing stellar luminosity/mass. Thus the stellar mass required is very sensitive to the adopted model. Additional simulations to test a stalled-shell scenario will be carried out in the near future.

There are several other possible factors contributing to the shortfall in stellar luminosity represented by our model. Some SCs blow their shells out of the disk and are not detected, some or perhaps even most OB stars do not form in SSCs, and perhaps earlier generations of stars will augment the FIR luminosity to some degree.

(4) Our model neglects the emission from the low density ambient ISM ($n_{ism} = 30\,\mathrm{cm}^{-3}$), due to the lack of knowledge of the structure of this component in a starburst galaxy, and to the lack of direct observational data of this gas component that could be used to distinguish this gas and its physical state from the shell emitting gas in our models. If the ambient medium were uniform, as assumed in the model, it would produce no observable emission, since the density is too low to excite even the first excited rotational level. If, however, the ambient gas is assumed to be highly non-uniform, as is more likely the case, we can use the

total mass adopted for the sampled volume to estimate its CO emission by simply using the X-factor for the CO emitting gas in our own Galaxy. We find that, before the shells form, the ^{12}CO(1-0) emission from this ambient gas component would be about 54% of the total current emission within the central 1 kpc region. Note however that at high-J, there may be only very weak emission from this ISM component. Hence, the consequence of adding the emission of this lower density ambient gas component to the model would be to reduce the apparent excitation of the combined emission, especially the lower-J transitions.

(5) A fixed microturbulent Doppler velocity ($\delta v_D = 1.5$ km s^{-1}) is used in our model, as a heating mechanism in the PDRs and as a broadening mechanism for the molecular line profile. However, the choice of turbulent velocity directly affects the computed CO line flux densities. In the optically thick case, the flux is directly proportional to the turbulent velocity, whereas in the optically thin case there is no dependence. Since the lower-J transitions are optically thick, more so than the higher level transitions, we anticipate that the use of a higher turbulent velocity would reduce the slope of the line SED (see Fig. 8).

(6) The assumption of the semi-infinite plane-parallel geometry in our PDR code is certainly a limitation, as the FUV intensity may be underestimated due to leakage of radiation from the region exterior to the cloud/shell, resulting in an increase in the local mean intensity at the edge of the slab. More advanced models of the shell geometry are simply beyond the scope of the PDR code at the time, and solving for the radiation field from both sides of the slab dramatically increases the computation time and would make the code too slow to run.

(7) Other effects will invalidate our model for later stages of shell evolution. For example, after 30 Myr the largest radius of the shells in our model ensemble is about 678 pc. Thus, it will be merged with other shells, an effect which is not included in the model. It will also have extended beyond the scale height of the disk (300 pc along the minor axis), and be subjected to shear due to differential galactic rotation. However, these problems occur at ages older than our CO best fit model, and they should not significantly affect our best fit result.

Overall, our analysis shows that the sub-mm/mm line emission reflects the recent star formation history in a starburst galaxy. The foregoing list of caveats and limitations ultimately limit the precision with which one can obtain a realistic age for the starburst by the method described in this paper. Some of the effects described lead to an underestimate and some to an overestimate. Thus, to some extent, the effects are liable to cancellation. However, the one factor upon which the ages depend most strongly is stellar evolution, since the evolutionary state of the cluster governs the flux of FUV emission incident upon the shell, and this in turn has an important influence on the SED of the molecular line emission.

A consequence is that the age is unlikely to be profoundly affected by the effects listed. This also means that there should be little surprise with the agreement with other methods. However, the total cluster mass responsible is exceptionally sensitive to the model for the expansion of the shell, and consequently this quantity is less well determined than the age. In our model, it appears likely that this stellar mass in our cluster ensemble is severely underestimated.

5. Conclusions

This paper presents a *first* attempt at addressing the question of whether there is a *signal* in the FIR/sub-mm/mm molecular and atomic line data of the phase of a starburst. By comparing our evolving starburst models with available data of nearby starburst galaxies, notably M 82, we show that it is possible to (1) successfully model the time-dependent FIR/sub-mm/mm line emission of molecular and atomic gas; (2) relate the observed molecular line properties of a starburst galaxy to its age, and hence to constrain the global star formation history; and (3) examine the possible relevance to the formation of the molecular rings in M 82.

In essence, we have provided a *complementary* study to the previous work on estimating the age(s) of starburst in M 82 using quite different methods. In particular, the method is analogous to that of Efstathiou et al. (2000), which considered the observable effects of an evolving cluster on the IR emission from the surrounding expanding dust shell. We have also provided support for the *hypothesis* of molecular ring formation in the center of M 82.

The main conclusions drawn from comparisons of our ESbM model with the observation are:

1. There is good agreement between our supershell kinematic model and the observations of the expanding supershell centered around the presumed supernova remnant SNR 41.9 + 58 in M 82. The agreement supports the *hypothesis* that this supershell is created by strong winds from a young star cluster with a total mass of 2.2 x 10^6 $M_\odot$ which formed at its center about 0.8 Myr ago, and the total mechanical energy needed for the creation of this supershell is about 1.5×10^{54} ergs. This is the energy equivalent of the winds associated with $\sim$ 1700 O stars (each with $m_* \geq 40$ $M_\odot$). Our model also shows that there should be excess CO emission at high excitation transitions in this supershell. This is consistent with the provisional detection of such excess emission at ^{12}CO(6-5) in the region of this supershell seen after the surrounding disk emission is removed. Both agreements suggest that the set of evolving starburst models we have put forward in this paper can be used to interpret other

shells in M 82 or shells in other starburst galaxies.

2. The *age* derived from our analysis of CO line SEDs and line ratio diagrams using an instantaneous burst model is 5 - 6 Myr for the central 1 kpc region, with most of the CO emission arising from the central 680 pc region. The age derived from our atomic data is slightly older (10 Myr) for a larger area (i.e. 1,2 kpc) We suggest that these two ages may be a result of sampling different regions. It is unclear from our analysis whether they refer to the same period of star forming activity or to two spatially separated independent bursts. A more sophisticated model and more data are needed to clarify the picture. We do note however that our extended starburst model result also shows that a uniform star formation rate over the past 10 Myr can also produce a satisfactory model fit to the ^{12}CO data. Hence, the star formation in M 82 can be either viewed as instantaneous burst occurred 5 - 6 Myr ago, or this epoch could represent a characteristic time about which recent star formation history is centered. These burst ages derived from our models are similar to the results found in optical and infrared studies. These results lead us to conclude that the observed FIR/sub-mm/mm line spectra of a starburst galaxy can be successfully modeled in terms of the evolutionary scheme of an GMC/shell ensemble, and such studies can usefully constrain the age(s) or star formation history of a starburst galaxy.

The starburst ages derived from our model are dependent on a great variety of assumptions, e.g. the initial upper mass limit of the cluster spectrum. We find that the model can provide acceptable fits to the data only if the dominant initiating starburst clusters are massive, at least 5×10^5 $M_\odot$, corresponding to a GMC mass of 2×10^6 $M_\odot$. The uncertainty of the derived age is also affected by many other model assumptions, and the effects of varying these assumptions have not been examined. These include, for example, the effect of including the CO emission (especially low-J transitions) from the lower density ambient ISM, the effect of including a higher cosmic-ray ionization rate, and the effect of increasing the shell microturbulent velocity. Some of these effects would lead to an underestimate and some to an overestimate of the age, and hence to some extent, these effects would be expected to cancel each other out. However, since the evolutionary state of the cluster governs the flux of FUV radiation incident upon the shell, and this in turn has a pronounced effect on the SED of the molecular line emission, the stellar evolution is a crucial factor in constraining the derived age. The starburst stellar mass and luminosity predicted by our models are significantly underestimated, based on a comparison with the observed FIR luminosity which is a factor of about twenty larger than our model value for the total luminosities of the clusters. Probable causes for this underestimate include (1) the neglect of the effects of the pressure exerted by the ambient gas, resulting in an overestimate of the shell radii; and (2) an overestimate of the supernova mechanical power which would also lead to an overestimate of the shell radii. Including these effects would allow more stellar luminosity

in the starburst for the mass of gas swept up in the shells required to match the CO data. Hence, the shortfall in our predicted stellar luminosity tends to support the widely held idea that bubbles/shells grow more slowly than the simple bubble theory predicts (Weaver er al. 1977; McCray & Kafatos 1987).

Our model also cannot provide a basis for incorporating higher density tracers (e.g. HCN and HCO^+), Because the critical densities are, for example, approximately 10^5 and 10^7 for the (1-0) and (4-3) transitions for both molecules. The HCO^+ intensities may be affected by cosmic-ray ionization when it becomes the dominant heating source in the gas. Both HCN and HCO^+ are associated with dense shells and their parent GMCs seen only at the earliest phase of the starburst evolution. But another principal source is required, most probably dense gas associated with the cores of potential star forming regions, not included in our model. If the dense cloud core component was included in our model, the effect of a higher cosmic-rate ionization rate (in M 82) should be taken into account.

3. The results of the model analysis described above (item 2), also yield insights into the total gas content and its structure. For example, the total H_2 gas mass ~ 2 - 3.4×10^8 $M_\odot$, is consistent with that measured independently in the center of M 82. The inference is that the neutral ISM and possibly the molecular ring in the center of M 82 are largely the products of evolving shells. However, our interpretation concerning the ring formation is not unique, and the rings may also be created by Linblad resonance instabilities associated with the gravitational effects of the bar.

I would like to thank my Ph.D. thesis advisor E. Seaquist for his guidance and support. I also thank J. Yates at UCL for discussions on the *SMMOL*, T. Bell at Caltech and S. Viti at UCL for discussions on the *UCL_PDR*, and C. Leitherer for discussions on the *Starburst99*. I am grateful to the Canadian Institute for Theoretical Astrophysics at University of Toronto for their generosity in allowing me to use their computing facility to run the PDR and Radiative Transfer simulations. I thank Space Telescope and Science Institute and National Radio Astronomy Observatory for kindly hosting me as their pre-doc visiting student. I also thank the referee for his careful reading, helpful comments, and his patience. This research was supported by a research grant from the Natural Sciences and Engineering Research Council of Canada to E. R. Seaquist, and a Reinhardt Graduate Student Travel Fellowship from the Department of Astronomy and Astrophysics at the University of Toronto.

REFERENCES

Bally, J., Stark, A. A., Wilson, R. W., & Henkel, C. 1988, ApJ, 324, 223

Barker, S., de Grija, R., & Cerviñs, M. 2008, A&A, 484, 711

Bartel, N., & Bietenholz, M. F. 2005, *AdSpR*, 35, 1057

Bastian, N., Gieles, M., Efremov, Yu. N., & Lamers, H. J. G. L. M. 2005, A&A, 443, 79

Bayet, E., et al. 2008, ApJ, 684, 35

Beck, S. C., Lacy, J. H., Baas, F., & Townes, C. H. 1978, ApJ, 226, 545

Bell, T. A. 2006, *Ph.D. Thesis*, University College London, UK

Bell, T. A., Viti, S., Williams, D. A., Crawford, I. A., & Price, R. J. 2005, MNRAS, 357, 961

Booth, R. S. & Aalto, S. 1998, in The Molecular Astrophysics of Stars and Galaxies, T. W. Hartquist & D. A. Williams (eds.), Oxford Science Publications, 437

Boselli, A., Lequeux, J., & Gavazzi, G. 2002, A&A, 384, 33

Brouillet, N., & Schilke, P. 1993, A&A, 277, 381

Carlstrom, J. E., & Kronberg, P. P. 1991, ApJ, 366, 422

Colbert, J. W. et al., 1999, ApJ, 511, 721

Dame, T. M., Elmegreen, B. G., Cohen, R. S., & Thaddeus, P. 1986, ApJ, 305, 892

de Grijs, R., O'Connell, R. W., & Gallagher, J. S., III 2001, AJ, 121, 768

de Jong, T. 1977, A&A, 55, 137

Dewangan, G. C., Titarchuk, L., & Griffiths, R. E. 2006, ApJ, 637, 21

Dopita, M. A. et al., 2005, ApJ, 619, 755

Efstathiou, A., Rowan-Robinson, M., & Siebenmorgen, R. 2000, MNRAS, 313, 734

Elmegreen, G. G., Lada, C. J., & Dickinson, D. F. 1979, ApJ, 230, 415

Fagotto, F., Bressan, A., Bertelli, G., & Chiosi, C. 1994, *A&AS*, 105, 29

Farquhar, P. R. A., Millar, T. J., & Herbst, E. 1994, MNRAS, 269, 641

Förster-Schreiber, N. M., Genzel, R., Lutz, D.,Kunze, D., & Sternberg, A. 2001, ApJ, 552, 544

Förster-Schreiber, N. M., Genzel, R., Lutz, D., & Sternberg, A. 2003, ApJ, 599, 193

Franco, J., Tenorio-Tagle, G., & Bodenheimer, P. 1990, ApJ, 349, 126

Galliano, F., et al. 2003, A&A, 407, 159

Gao, Y., Lo, K. Y., Lee, S.-W., & Lee, T.-H. 2001, ApJ, 548, 172

García-Burillo, S., Martín-Pintado, J., Fuente, A., & Neri, R. 2001, ApJ, 563, 27

Glover, S. C. O., & Mac Low, M. 2007, ApJ, 659, 131

Goldreich, P. & Kwan, J. 1974, ApJ, 189, 441

Gusten, R., et al. 1993, ApJ, 402, 537

Hollenbach, D. J. & Tielens, A. G. G. M. 1997, ARA&A, 35, 179

Jog, C. J., & Solomon, P. M. 1992, ApJ, 387, 152

Kawakatu, N., & Umemura, M. 2005, ApJ, 628, 721

Kennicutt, R. C., Jr. 1998, ApJ, 498, 541

Keto, E., Ho, L. C., Lo, K.-Y. 2005, ApJ, 635, 1062

Leitherer, C. et al., 1999, ApJS, 123, 3

Leitherer, C., 2005, *AIPC*, 783, 280

Lipscy, S. J., & Plavchan, P. 2004, ApJ, 603, 82

Lo, K. Y., et al. 1987, ApJ, 312, 574

Lord, S. D., Hollenbach, D. J., Haas, M. R., & Rubin, R. H. 1996, ApJ, 465, 703

Lynds, C. R., & Sandage, A. R. 1963, ApJ, 137, 1005

Mac Low, M. M., & McCray, R. 1988, ApJ, 324, 776

Mao, R. Q., et al. 2000, A&A, 358, 433

Mathis, J. S., 1990, ARA&A, 28, 37

McCray, R. & Kafatos, M. 1987, ApJ, 317, 190

Melo, V. P., Muñoz-Tuñón, C., Maíz-Apellániz, J., & Tenorio-Tagle, G. 2005, ApJ, 619, 270

Negishi, T., Onaka, T., Chan, K.-W., & Roellig, T. L. 2001, A&A, 375, 566

Neininger, N., t al. 1998, A&A, 339, 737

Oey, M. S., & García-Segura, G. 2004, ApJ, 613, 302

Pedlar, A., Muxlow, T., & Wills, K. A. 2003, *RMxAC*, 15, 303

Petitpas, G. R., & Wilson, C. D. 2000, ApJ, 538, 117

Petitpas, G. R., & Wilson, C. D. 2001, *ESASP*, 460, 483

Rieke, G. H., Lebofsky, M. J., Thompson, R. I., Low, F. J., & Tokunaga, A. T. 1980, ApJ, 238, 24

Rieke, G. H., Loken, K., Thompson, M. J., & Tamblyn, P. 1993, ApJ, 412, 99

Rawlings, J. M. C., & Yates, J. A. 2001, MNRAS, 326, 1423

Rieu, N. Q., Nakai, N., Jackson, J. M. 1989, A&A, 220, 57

Röllig, M., et al. 2007, A&A, 467, 187

Salpeter, E. E. 1955, ApJ, 121, 161

Sanders, D. B., Scoville, N. Z., & Solomon, P. M. 1985, ApJ, 289, 373

Satyapal, S., et al. 1999, ApJ, 483, 148

Shen, Jianjun, & Lo, K. Y. 1996, *IAUS*, 170, 101

Seaquist, E. R., Frayer, D. T., & Bell, M. B. 1998, ApJ, 507, 745

Seaquist, E. R., & Frayer, D. T. 2000, ApJ, 540, 765

Seaquist, E. R., Lee, S. W., & Moriarty-Schieven, G. H. 2006, ApJ, 638, 148

Siebenmorgen, R., & Krügel, E. 2007, A&A, 461, 445

Silich, S., Tenorio-Tagle, G., & Muñoz-Tuñón, C. 2007, ApJ, 669, 952

Smith, L. J., et al. 2006, MNRAS, 370, 513

Solomon, P. M., Rivolo, A. R., Barrett, J., & Yahil, A. 1987, ApJ, 319, 730

Stutzki, J. et al. 1997, ApJ, 477, 33

van Zadelhoff, G. J. et al., 2002, A&A, 395, 373

Vazquez, G. A., & Leitherer, C. 2005, ApJ, 621, 695

Visvanathan, N. 1974, ApJ, 192, 319

Walter, F., Weiss, A., & Scoville, N. 2002, ApJ, 580, 21

Ward, J. S., Zmuidzinas, J., Harris, A. I., & Isaak, K. G. 2003, ApJ, 587, 171

Weaver, R., McCray, R., Castor, J., Shapiro, P., & Morre, R. 1977, ApJ, 218, 377

Weiss, A., Walter, F., Neininger, N., & Klein, U. 1999, A&A, 345, 23

Weiss, A., Neininger, N., Hüttemeister, S., & Klein, U. 2001, A&A, 365, 571

Weiss, A., Walter, F., & Scoville, N. Z. 2005, A&A, 438, 533

Weliachew, L., Fomalont, E. B., & Greisen, E. W. 1984, A&A, 137, 335

Wild, W. et al., 1992, ApJ, 265, 447

Wills, K. A., Redman, M. P., Muxlow, T. W. B., & Pedlar, A. 1999, MNRAS, 309, 395

Wills, K. A., Das, M., Pedlar, A., Muxlow, T. W. B., & Robinson, T. G. 2000, MNRAS, 316, 33

Wills, K. A., Pedlar, A., & Muxlow, T. W. B. 2002, MNRAS, 331, 313

Wilson, C., et al. 2008, *ApJS*, 178, 189

Young, J. S., & Scoville, N. Z. 1984, ApJ, 287, 153

Yao, Lihong 2009, *Ph.D. Thesis*, University of Toronto, Canada (Yao Thesis).

Yao, Lihong 2009, *ApJ*, submitted (Paper III).

Yao, Lihong, Seaquist, E. R., Kuno, N., & Dunne, L. 2003, ApJ, 588, 771

Yao, Lihong, Bell, T., Viti, S., Yates, J. A., & Seaquist, E. R. 2006, ApJ, 636, 881 (Paper I)

Yun, M. S., Ho, P. T. P., & Lo, K. Y. 1993, ApJ, 411, 17

This preprint was prepared with the AAS LaTeX macros v5.2.

Table 3. Model parameters and variables

Models	Description
Independent Variable:	time or starburst age t
Dependent Variables:	shell radius R_s, expansion velocity V_s, number density n_s, and thickness d_s
	gas (kinetic) temperature T_{gas}, dust (thermal) temperature T_{dust}
	chemical abundances of different molecules and atoms in the shell
	number densities of collisional partners H, e^-, H+, p-H_2, o-H_2, and He
Fixed Parameters:	GMC mass M_{GMC}: 3.16 × 10^3 - 10^7 $M_\odot$
	stellar mass m_*: 0.1 - 120 $M_\odot$
	star formation efficiency (SFE) $\eta = 0.25$ for *Winds*, $\eta = 1.0$ for *post-SN*
	metallicity $\mathcal{Z} = 1.0$ $Z_\odot$
	gas-to-dust ratio = 100
	ambient ISM density of each shell n_{ism} (parent GMC at *Winds*, 30 cm^{-3} at *post-SN*)
	microturbulent velocity $\delta v_D = 1.5$ km s^{-1}
Fitting Parameters:	total gas mass of the ensemble M_{total}, burst age t
Outputs:	line profiles for each transition in each molecules and atoms
	integrated line intensity or flux